J. Fluid Mech. (2000), *vol.* 409, *pp.* 185–221. Printed in the United Kingdom

The effect of rotation on vertical Bridgman growth at large Rayleigh number

By M. R. FOSTER

Department of Aerospace Engineering, Applied Mechanics and Aviation,
The Ohio State University, Columbus, OH 43210, USA

(Received 15 January 1999 and in revised form 24 July 1999)

Convection effects in the melt of a vertical Bridgman furnace, used for solidifying a dilute binary alloy, are known to cause significant, and undesirable, non-uniformity in the alloy. We have found previously that non-axisymmetry significantly degrades the performance of the furnace at large Rayleigh number, Ra, and small Biot number, $\mathscr{B}$. There have been a number of studies on improvement of the alloy quality by the introduction of additional forces into the melt flow – magnetic forces or d'Alembert forces due to various sorts of acceleration of the ampoule. In this paper, we explore the effects on the radial segregation generated by rotating the ampoule about its vertical axis. We determine that the magnitude of segregation is proportional to the product of $\mathscr{B}$ and the thickness of the thermal layer on the crystal–melt interface. As the rotation, as measured by a Taylor number, $\mathscr{T}$, increases beyond $O(Ra^{1/3})$, the thermal layer thickens and so the segregation increases. Finally, at $\mathscr{T} = O(Ra^{1/2})$, the thermal adjustment occurs on outer scales, and hence the solutal concentration increases to $O(\mathscr{B})$. Hence rotation about the vertical axis actually degrades performance!

1. Introduction

In two previous papers (Foster 1997, 1999) we considered the steady-state operation of a vertical Bridgman apparatus for processing a dilute binary alloy, in the case when either the thermal or Rayleigh number is large, and also the Biot number is small. The two-dimensional (and axisymmetric) analysis of the first paper was extended in the second to include effects of azimuthally varying heating at the sidewall. In both cases, we theoretically verified what has already been found in both experiment and theory (see, for example, Adornato & Brown 1987; Xiao *et al.* 1966; and Tanveer 1994): the radial distribution of the dopant in the other metal is highly non-uniform, lessening the usefulness of the product. Such furnaces are also utilized for single-component materials, but the detailed asymptotic results given below are not relevant to that case. No doubt similar asymptotic methods can be used for such a single-component situation as well, but the concentration field is intimately connected to the thermal and velocity fields in most of the parameter ranges of this paper, and so no simple limit of the results can be used to generate results for the no-solute case.

To first set the geometrical configuration, figure 1 is a schematic of a radial section of the furnace. The ampoule has radius a, with the radial coordinate made dimensionless with that quantity. The coordinate system is chosen so that the crystal–melt interface is located at $z = 0$ for the idealized one-dimensional case, when there is no heat flux through the boundaries. With heat transfer, the interface is at $z = Z(r, \theta)$, so the melt occupies that region above $z = Z$, and the solid below. The overall temperature

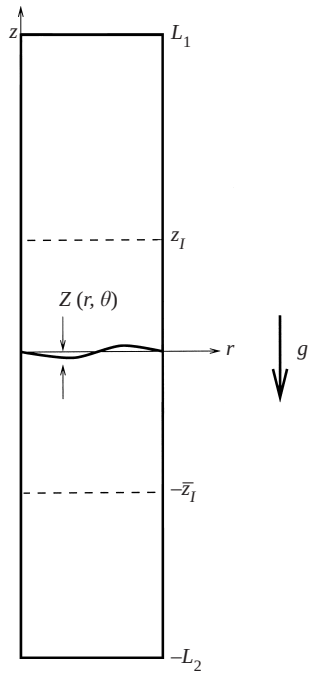

FIGURE 1. Geometrical configuration of the furnace.

difference in the furnace, from $z = L_1$ to $z = -L_2$, is denoted by ΔT. Heat is transferred through the sidewalls for $z > z_I$ and $z < -\bar{z}_I$; the region between is taken to be perfectly insulated. The two parameters whose magnitudes primarily govern the performance of this device are the Rayleigh number, and the Biot number, defined as

$$Ra = \frac{g\alpha\Delta T a^3}{\kappa\nu}, \quad \mathscr{B} = \frac{ha}{k}, \tag{1.1}$$

where ν and κ are the kinematic viscosity and thermal diffusivity of the melt, and k is its thermal conductivity; h is the convection coefficient at the outer wall of the ampoule. There is also a solutal Rayleigh number defined later which is not as important to the work presented here. Foster (1997, 1999) shows that for large Ra, the non-uniformity in the dopant concentration scales with $\mathscr{B}Ra^{-1/6}$. The choice of Biot number and the question of conduction through the ampoule wall is deferred until the discussion of boundary conditions in § 2.

Moon, Kim & Ro (1997) and Weber, Neumann & Müller (1990), among others, have suggested that some procedure for stirring the melt should result in more homogeneity in the crystal. In this paper, we examine one such idea: stirring the melt by means of Coriolis forces due to the rigid rotation of the ampoule about its vertical axis. Both experiments and some prior theoretical work indicate that not only does the radial segregation improve, but the onset of interfacial instability is delayed to larger pulling speeds with the addition of rotation (Weber *et al.* 1990). However, some more recent numerical work, by Lee & Pearlstein (1998), indicates that if the rotation axis is aligned with gravity, then the rotation actually makes segregation worse. Before proceeding to the analysis, we review briefly the qualitative features of the zero-rotation results. More details may be found in Foster (1999).

In everything that follows in this paper, we shall be exploring the 'thermally

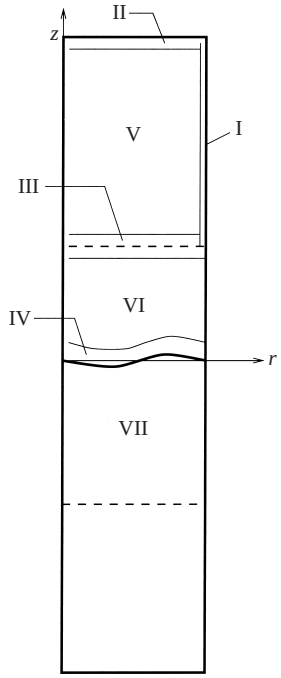

FIGURE 2. Schematic of the flow field.

dominant' case, for which the thermal Rayleigh number in (1.1) is much larger than a solutal Rayleigh number.

1.1. *Synopsis of the zero-rotation Bridgman furnace*

The flow field for a non-rotating furnace, as deduced by Foster (1997, 1999), is shown in schematic form in figure 2. The flow is driven by heat transfer through the sidewall, which causes fluid to rise in the boundary layer, Region I, whose width scales as $Ra^{-1/4}$. Thinking for the moment solely of the meridional circulation in the ampoule, the upwardly moving fluid enters the layer of thickness $Ra^{-1/6}$ at the top, Region II, and then sinks out of that layer into the interior, Region V, closing the circulation by a return flow into the edge of the Region I boundary layer, or first into the horizontal shear layer, Region III, and then into I. Because of the insulating condition along the boundary of Region VI, there is no sidewall boundary layer and hence the flow in that zone is much weaker. Azimuthal variations in the sidewall heating cause the inflow from V to I to vary with azimuth angle, and therefore leads to a swirling flow, superposed on the meridional angularly-averaged eddy. Because of the insulating zone around the crystal–melt interface, it is well known that this 'upper eddy' is isolated from the interface (Ardonato & Brown 1987). The most intense motion is in Region IV – the 'lower eddy'; it is due to heat flux at the interface from the solid, Region VII. Since the flux does not match the flux from above, the interface deflects, thereby inducing a buoyancy-driven flow. The result of that interaction at the interface is the concentration variation noted above.

Figure 3 shows contours of constant radial velocity on two different azimuthal planes in the melt, for the case of an ampoule subjected to azimuthally varying sidewall heating, as computed by Foster (1999); parameters listed in the caption are defined in the next section. One can clearly see the boundaries of the upper eddy,

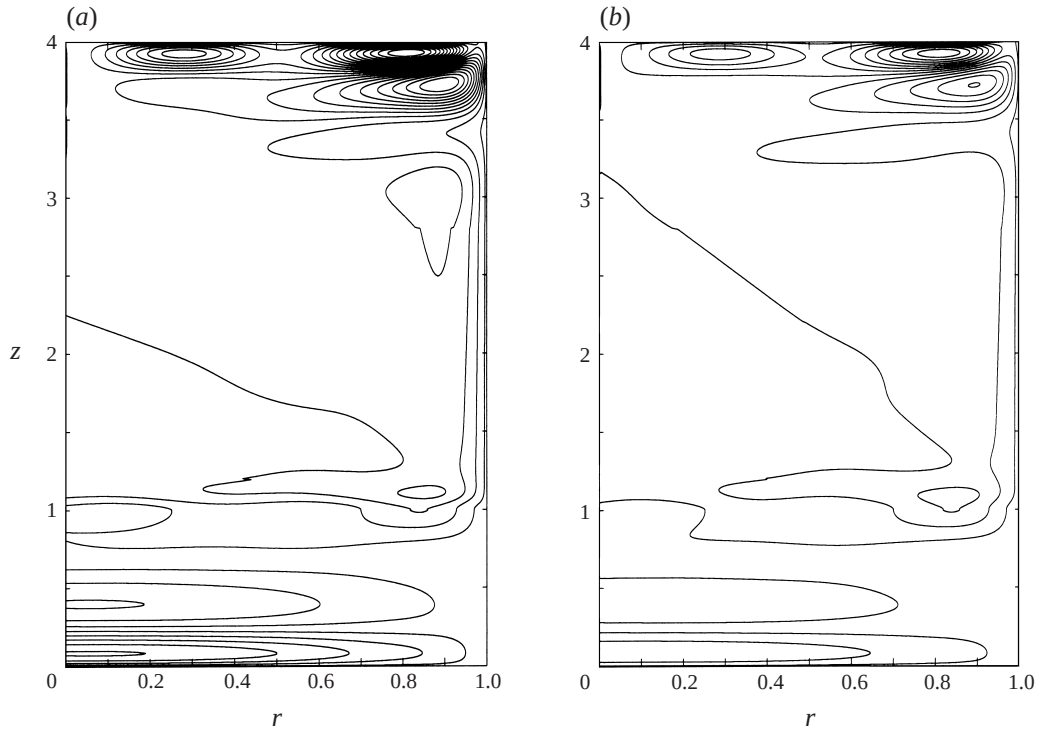

FIGURE 3. Lines of constant dimensionless radial velocity component for $Pe' = 0.1$, $Ra = 10^6$, $k = 0.5$, $M = -1$, $G = -1$, $\mathscr{K} = 1$, $\Gamma = 0$, $L_1 = L_2 = 4$, $z_I = \bar{z}_I = 1$ for sections at (*a*) $\theta = 0$ and (*b*) $\theta = 60°$. There are 25 equal intervals between values of -7.9×10^{-5} and 8.1×10^{-5}. Heating has a $\cos\theta$ variation.

and what is a relatively weak – at this relatively small Rayleigh number – lower eddy near the interface. At the relatively small Rayleigh number for this figure, the lower eddy is not as intense as the upper one – something that changes for $Ra \to \infty$.

As we shall see in the next section, at sufficiently small Biot number, $\mathscr{B}$, the Navier–Stokes equations, associated transport equations and boundary conditions constitute a linear problem. In such a case, it is generally convenient to split the sidewall heating into an azimuthally averaged segment, and an azimuthally varying component with zero average. Linearity of course means that the same split may be done for the velocity vector and thermodynamic quantities. So, for some generic quantity ψ, for example,

$$\psi(r,\theta,z) = \langle\psi\rangle(r,z) + \tilde{\psi}(r,\theta,z), \quad \langle\psi\rangle \equiv \frac{1}{2\pi}\int_0^{2\pi} \psi(r,\theta,z)\,\mathrm{d}\theta, \tag{1.2}$$

where (r,θ,z) are the usual circular polar coordinates. It is evident, then, that

$$\langle\tilde{\psi}\rangle \equiv 0. \tag{1.3}$$

1.2. *Overview of flow changes with Taylor number*

The work here builds on that of Foster (1997, 1999), who found, among other things, that the interfacial deflection, Z, scales as $\mathscr{B}Ra^{-1/6}$ in the absence of rotation. It is

convenient to measure the rotation of the ampoule by a Taylor number,

$$\mathscr{T} \equiv \frac{\Omega a^2}{\nu}, \tag{1.4}$$

where Ω is the rotation rate of the ampoule, a is the ampoule radius and ν is the kinematic viscosity in the melt. The nature of the melt flow and the segregation then depends strongly on the relative sizes of $\mathscr{T}$ and the other dimensionless parameters of the problem, particularly the Rayleigh number. We summarize below the changes in the flow and solidification with Taylor number, before proceeding to all of the mathematical details. Each case is also labelled with the number of the section in the paper in which that parameter range is explored.

Section 4: $\mathscr{T} = O(1)$. There is no deviation from the $\mathscr{T} \equiv 0$ interfacial scalings. The motion in the melt is slightly altered, however, a harbinger of what is to come: Coriolis-driven swirl motion arises, and the vertical vorticity component is now non-zero, for both $\langle \psi \rangle$ and $\tilde{\psi}$.

Section 5: $1 \ll \mathscr{T} \ll Ra^{1/3}$. In this range, the interfacial deflection and material segregation do not alter in scale, though the flow structure does change a bit, reflecting increased effects of swirl, for example.

Section 6: $\mathscr{T} = O(Ra^{1/3})$. We examine this case for axisymmetry only. The interfacial boundary layer is more complicated here, with Coriolis effects playing an important role in the layer for the first time, but the qualitative role of the layer is unchanged. Hence, $\langle Z \rangle = O(\mathscr{B} Ra^{-1/6})$ as above. Details of the melt flow are again somewhat altered, but without an effect on $\langle Z \rangle$. There is an indication in the result that at still larger values of $\mathscr{T}$ the segregation will be larger.

Section 7: $Ra^{1/3} \ll \mathscr{T} \ll Ra^{1/2}$. Exploring the azimuthally varying situation only here, we find that $\tilde{Z}$ is now larger than in the cases for smaller $\mathscr{T}$, namely $\tilde{Z} = O(\mathscr{B}\mathscr{T}/Ra^{1/2})$. The reason is that the interfacial layer, Region IV in figure 2, splits into a thinner Ekman layer in which speed adjustments occur, and a thicker thermal layer, whose width is $\mathscr{T}/Ra^{1/2}$.

Section 8: $\mathscr{T} = O(Ra^{1/2})$. At this stage, considering axisymmetric situations only, rotation appears counter-productive. The interfacial boundary layer is simply an Ekman layer. Increased Coriolis force magnitudes have caused the thermal adjustments to occur in Regions V and VI rather than in Region IV. Thus, at this stage, the axisymmetric interfacial deflection, $\langle Z \rangle$, increases to $O(\mathscr{B})$.

Section 9: $\mathscr{T} = O(Ra)$. In this final parameter range, the flow is fully rotation-dominated. The order of $\langle Z \rangle$ remains $\mathscr{B}$ as for the above case. The flow structure, however, is quite different from the previous regime – with radial motion strongly suppressed and a vertical drift velocity driven by Ekman entrainment requirements in Regions II and IV. Further increases in rotation would appear to be futile, in terms of reducing segregation.

Since so many parameter ranges are examined here, two simplifications in presentation have been made to minimize the size of the paper. First, as may be noted in the above discussion, both axisymmetric and non-axisymmetric cases are not presented in detail in each parameter range. Secondly, all of the solution details are not given in every parameter range, but generally only in ranges for which the solutions depart significantly from those already given by the author (Foster 1997, 1999).

1.3. *The rotating flow foundations*

Foster (1999) has already pointed out that there are great physical and hence mathematical complexities of a flow like that described here at locations where

boundary layers intersect, as for example at the junction of Regions I and III in figure 2. Fortunately, the boundary-layer structure in these solidifying fluids is nearly identical with the layers of rapidly-rotating flow theory – except that everything is turned through 90°. Though much groundwork for these rotating flows was laid by Stewartson (1966), it is the paper by Moore & Saffman (1969) that shows how to deal properly with these layer-intersection problems. For example, as the fluid in the Region III layer arrives at the outer wall ($r = 1$), it flows into what is effectively a point sink on that scale – since the non-uniformities in the sidewall layer are on a vertical scale $Ra^{-1/4}$, which is $o(1)$ on the Region III scale. Because all of that has been worked out for the very similar rapidly-rotating flow problems by Stewartson and Moore & Saffman, there is no need to examine those issues here. The interested reader should refer to the works cited for details.

2. Formulation

We consider here a Bridgman-type furnace, through which a circular ampoule of melt moves at a steady speed V. In the analysis below, the ampoule translates in the $-z^*$-direction, in the same direction as the gravitational acceleration. We utilize a coordinate system in which the propagating solidification front is stationary. (See figure 1.) Let (r^*, θ, z^*) be the usual cylindrical polar coordinates, and let the thermal and solutal conditions be imposed at $z^* = aL_1$, where the temperature is taken to be T_H, and at $z^* = -aL_2$, where $T^* = T_C$, with $T_H > T_C$; a is the radius of the ampoule. (The starred quantities are dimensional.) We choose the coordinate-system origin so that the nominal crystal–melt interface (that is, with perfect sidewall insulation) is located at $z^* = 0$. We recalled in the previous paper (Foster 1999) the results of Tiller *et al.* (1953) that the thermal and solutal distributions variation with z under perfect insulation conditions are given by

$$T^* = T_s^* + \frac{\mathscr{K}\Delta T z}{L_2 + \mathscr{K}L_1}, \quad z > 0, \tag{2.1}$$

$$T^* = T_s^* + \frac{\Delta T z}{L_2 + \mathscr{K}L_1}, \quad z < 0, \tag{2.2}$$

$$T_s^* = \frac{\mathscr{K}L_1 T_C + L_2 T_H}{\mathscr{K}L_1 + L_2}, \tag{2.3}$$

$$c^* = c_\infty \left(1 + \frac{1-k}{k} \mathrm{e}^{-Pe' z}\right), \tag{2.4}$$

where $T_s^* \equiv T_M^* - mc_\infty/k$ is the surface temperature; $\mathscr{K}$ is the ratio of the thermal conductivities in the solid and the melt, respectively; c^* is the concentration of the (dilute) solute; k is the 'segregation coefficient'; and Pe' is the solutal Péclet number, Va/D, with D the solutal diffusion coefficient. The coordinates r and z are made dimensionless with the ampoule radius, a. The linear thermal distribution follows from an assumption that the thermal Péclet number is very small.

2.1. *Equations of motion and parameters*

To explore modifications to this one-dimensional distribution due to imperfect sidewall insulation or other effects coupled with effects of rigid rotation of the furnace, we follow Foster (1997) in writing the fluid velocity vector as $\boldsymbol{u}^* = -V\boldsymbol{k} + (g\alpha\Delta T a^2/\nu)\mathscr{B}\boldsymbol{u}$, where $\Delta T = T_H - T_C$, α is the coefficient of thermal expansion and $\mathscr{B}$ is the Biot

number defined earlier, which is in fact driving the three-dimensional motion. We also write $T^* = \Delta T\, T_0(z) + \mathscr{B}\Delta T\, T$ and $c^* = \Delta c^*(C_0(z) + \mathscr{B}c/G)$, where $\Delta c^* C_0(z)$ is given by (2.4) and for convenience, we have taken $\Delta c^* \equiv c_\infty/k$. Substitution into the Boussinesq-approximated Navier–Stokes equations gives the following:

$$\nabla \cdot \boldsymbol{u} = 0, \tag{2.5}$$

$$Pr^{-1} Ra \mathscr{B}(\boldsymbol{u}\cdot\nabla)\boldsymbol{u} + 2\mathscr{T}\boldsymbol{k}\times\boldsymbol{u} + \nabla p = \nabla^2\boldsymbol{u} + \boldsymbol{k}(T+c), \tag{2.6}$$

$$\nabla^2 T = Raw T_0'(z) + \mathscr{B}Ra(\boldsymbol{u}\cdot\nabla)T, \tag{2.7}$$

$$\nabla^2 c = \frac{GRa}{\mathscr{E}} w C_0'(z) - Pe'\boldsymbol{k}\cdot\nabla c + \mathscr{B}\frac{Ra}{\mathscr{E}}(\boldsymbol{u}\cdot\nabla)c, \tag{2.8}$$

where $\boldsymbol{k} = \nabla z$ and velocity vector has components $\boldsymbol{u} = (u, v, w)$ in the radial, azimuthal (θ) and z directions respectively. Recall that the thermal Péclet number has already been taken to be very small, so terms involving that parameter have already been dropped. Three additional parameters, beyond those already noted, arise, namely the Prandtl number, Pr; a ratio of solutal-to-thermal diffusion, $\mathscr{E} \equiv D/\kappa$; and the quantity $G \equiv \beta\Delta c^*/(\alpha\Delta T)$. In addition to the thermal Rayleigh number Ra already defined, there is a Rayleigh number related to the density difference due to concentration variation, Ra_c, which is most conveniently written as $Ra_c = RaGPe'/\mathscr{E}$. Note that $Ra_c < 0$, since $G < 0$ for the heavy solute considered in this paper. In the solid, where we are ignoring vertical variation in solute concentration, c, the dimensionless temperature satisfies a zero-Péclet-number heat conduction equation,

$$\nabla^2 \bar{T} = 0. \tag{2.9}$$

As in the previous analyses, ignoring thermal Péclet number, required for the validity of (2.1), (2.2) and (2.9), implies that

$$\mathscr{E}Pe' = O(1). \tag{2.10}$$

However, we take the solutal Péclet number, Pe', and the Prandtl number, Pr, to be $O(1)$. Throughout this paper, we explore the 'thermally dominant' situation for which

$$Ra \gg |Ra_c| \Longrightarrow \frac{GPe'}{\mathscr{E}} \ll 1. \tag{2.11}$$

The rotation of the ampoule, undertaken to improve the quality of the crystal, introduces the Taylor number, $\mathscr{T}$, whose order relative to Ra determines the nature of the flow in the melt and the segregation in the solid. Note that in equation (2.6) the centrifugal term has been neglected. That amounts to ignoring the tilting of the iso-pycnyl surfaces due to the rotation of the ampoule. (To be consistent with the Boussinesq approximation, the centrifugal force cannot in this situation be absorbed into the pressure, since the density multiplier makes the force non-conservative.) In dimensionless terms, that leads to a restriction on the Taylor number,

$$(\alpha\Delta T Pr)^{1/2}\mathscr{T} \ll Ra^{1/2}. \tag{2.12}$$

This particular requirement is not very severe, since the Prandtl number is typically quite small for materials of interest. More precise orderings of $\mathscr{T}$ relative to Ra will be discussed below. Overturning of the fluid is avoided by requiring that $T_0'(z) + (G/\mathscr{E})C_0'(z) > 0$ for all z.

2.2. *Boundary conditions*

The boundary conditions to be imposed at the (as yet) unknown crystal–melt interface (at $z = Z(r,\theta)$) may be found in Brattkus & Davis (1988), or Tanveer (1994), and are

$$\boldsymbol{u} = \boldsymbol{0}, \tag{2.13}$$

$$T_0 + \mathscr{B}T = \bar{T}_0 + \mathscr{B}\bar{T} = T_M + M\left(C_0 + \frac{\mathscr{B}}{G}c\right) + \mathscr{B}\Gamma\frac{\nabla_h^2 Z}{(1+|\nabla Z|^2)^{3/2}}, \tag{2.14}$$

$$\frac{\partial(T_0 + \mathscr{B}T)}{\partial n} = \mathscr{K}\frac{\partial(\bar{T}_0 + \mathscr{B}\bar{T})}{\partial n}, \tag{2.15}$$

$$\frac{\partial(G\,C_0 + \mathscr{B}c)}{\partial n} = (k-1)(GC_0 + \mathscr{B}\,c)Pe', \tag{2.16}$$

at $z = Z(r,\theta)$, where n is a direction normal to the interface and ∇_h^2 is an horizontal Laplacian. The morphological number is $M \equiv -m\Delta c^*/\Delta T$; the dimensionless melting temperature T_M is equal to $T_M^*/\Delta T$, and Γ is a non-dimensional measure of the surface tension, with a factor $\mathscr{B}$ removed.

Boundary conditions are taken to be steady on the endwalls of the ampoule, so

$$T = 0, \quad c = 0, \quad \boldsymbol{u} = \boldsymbol{0} \quad \text{at } z = L_1, \tag{2.17}$$

$$T = 0 \quad \text{at } z = -L_2. \tag{2.18}$$

The validity of such end conditions in leading to a quasi-steady flow is discussed by Jalics (1998).

2.2.1. *Sidewall boundary conditions*

After substitution of the temperature expansion into Newton's law of cooling at the sidewall, the thermal boundary condition becomes

$$\left.\begin{aligned} \frac{\partial T}{\partial r} &= -\Theta(\theta)(T_0(z) - T_a) \quad \text{on } r = 1 \quad \text{for } z > z_I, \\ \frac{\partial \bar{T}}{\partial r} &= -\mathscr{K}^{-1}\overline{\Theta}(\theta)(\bar{T}_0(z) - \bar{T}_a) \quad \text{on } r = 1 \quad \text{for } z < -\bar{z}_I, \end{aligned}\right\} \tag{2.19}$$

$$\frac{\partial T}{\partial r} = 0 \quad \text{on } r = 1 \quad \text{for } -\bar{z}_I < z < z_I, \tag{2.20}$$

The quantities $T_a, \bar{T}_a \equiv T_a^*/\Delta T, \bar{T}_a^*/\Delta T$ are dimensionless measures of the ambient temperatures in the air outside the ampoule, in the hot and cool zones respectively. The quantities $\Theta(\theta)$ and $\overline{\Theta}$ allow for the possibility of azimuthal variations in the heat transfer into the ampoule. The h in the Biot number definition in (1.1) is chosen so that $\langle\Theta\rangle = \langle\overline{\Theta}\rangle \equiv 1$. For convenience in what follows, we denote the entire right-hand side of (2.19)–(2.20) by $f(z,\theta)$, noting that in this situation, f is always piecewise linear in z.

Before proceeding, we note that boundary conditions (2.19), (2.20) are written down assuming that the thermal conditions are imposed directly at the fluid or crystalline boundary. Of course, that is not the case; there is an ampoule wall through which the heat is conducted. Elementary one-dimensional analysis shows that, provided the ampoule wall is thin, these conditions are correct; all that one must do is replace the Biot number, $\mathscr{B}$, by a modified Biot number, namely,

$$\frac{\mathscr{B}}{1 + \mathscr{B}_a} \equiv \mathscr{B}' \longrightarrow \mathscr{B}, \tag{2.21}$$

where $\mathscr{B}_a$ is a Biot number associated with the ampoule wall, $\mathscr{B}_a \equiv hd/k_a$, if k_a is the thermal conductivity of the wall, which has thickness d. So long as this modified Biot number, $\mathscr{B}'$, is small, all of the analysis goes through unchanged with $\mathscr{B}'$ replacing $\mathscr{B}$. (It is interesting to note that $\mathscr{B}'$ might be small even if $\mathscr{B}$ is not – should $\mathscr{B}_a$ be large.) The extension to this situation with a wall of finite thickness requires, too, that the discontinuity in f ($\bar{f}$) at $z = z_I$ ($z = \bar{z}_I$) is preserved across the wall material. That will be the case if any 'spreading' of the discontinuity is small compared to the thickness of the Region III layer as it hits the wall, that is

$$\frac{d}{a} \ll z_I Ra^{-1/6}. \tag{2.22}$$

Hence, in summary, satisfaction of this condition and the replacement (2.21) together account for the presence of an ampoule wall.

In much of what follows, it is convenient to represent the sidewall heating as a Fourier series, hence we write

$$f(z,\theta) = \mathrm{Re}\left[\sum_{m=0}^{\infty} a_m(z)\mathrm{e}^{\mathrm{i}m\theta}\right], \tag{2.23}$$

with a similar series in the solid for $\bar{f}$.

No slip of fluid velocity and no transport of solute at the sidewalls means that

$$\boldsymbol{u} = \boldsymbol{0} \quad \text{on} \quad r = 1, \quad \text{all} \quad z. \tag{2.24}$$

and

$$\frac{\partial c}{\partial r} = 0 \quad \text{on} \quad r = 1, \quad \text{all} \quad z. \tag{2.25}$$

There are also obvious symmetry conditions on the centreline of the ampoule, at $r = 0$.

2.3. *The sidewall boundary layer*

As in Foster (1997, 1999), the motion in the melt is driven by heat transfer through the non-insulated portions of the sidewalls, reflected mathematically in the Newton's law of cooling boundary condition (2.20): the heat transfer induces a buoyant motion in a wall boundary layer of width $Ra^{-1/4}$, and so long as $\mathscr{B}$ is sufficiently small and

$$Ra^{-1/4}Pe' \ll 1,$$

a linear structure is appropriate to the layer, and so the velocity, thermal and solute distributions may be written down exactly. That results in simple formulae for boundary-layer entrainment as well as thermal (or solutal) edge conditions. These conditions essentially provide compatibility conditions at the 'wall' of the interior solutions. Here, for sufficiently large Taylor number, $\mathscr{T}$, the boundary-layer structure changes and hence the overall flow will be significantly modified.

Doing the usual boundary-layer approximations on equations (2.6)–(2.8), we have

$$p_r = 2\mathscr{T}v, \quad p_\theta + 2\mathscr{T}u = v_{rr}, \quad p_z = w_{rr} + T + c, \tag{2.26}$$

$$T_{rr} = RaT_0'w, \quad c_{rr} = \frac{GRa}{\mathscr{E}}C_0'(z)w. \tag{2.27}$$

These equations may be combined, with continuity, into two equations for w and v,

namely

$$w_{rrrr} + Ra\left(T_0' + \frac{G}{\mathscr{E}}C_0'(z)\right)w = 2\mathscr{T}v_{rz}, \tag{2.28}$$

$$v_{rrr} = -2\mathscr{T}w_z. \tag{2.29}$$

These equations may be combined into a single equation,

$$w_{rrrrrr} + Ra\left(T_0' + \frac{G}{\mathscr{E}}C_0'(z)\right)w_{rr} + 4\mathscr{T}^2 w_{zz} = 0. \tag{2.30}$$

There are clearly a number of differing limiting cases, depending on the relative orders of Ra and $\mathscr{T}$. If we use the scaling of Foster (1997, 1999) for the non-rotating cases, then we write $r - 1 = Ra^{-1/4}\xi$, and we recover the non-rotating equation,

$$w_{\xi\xi\xi\xi} + \left(T_0' + \frac{G}{\mathscr{E}}C_0'(z)\right)w = 0 \quad \text{for } \mathscr{T} \ll Ra^{3/4}. \tag{2.31}$$

In this case, the swirl velocity is decoupled, and found by subsequently integrating

$$v_{\xi\xi\xi} = -2\frac{\mathscr{T}}{Ra^{3/4}}w_z, \tag{2.32}$$

from which it is immediately evident from the restriction in (2.31) that v is an order of magnitude smaller than the vertical velocity component, w. What emerges, in the 'thermally dominant' regime considered in this paper are the formulae for edge conditions,

$$c_r = -\frac{GC_0'(z)}{\mathscr{E}T_0'(z)}f(z,\theta), \tag{2.33}$$

and

$$u = \frac{\partial}{\partial z}\left(\frac{f(z,\theta)}{Ra\,T_0'(z)}\right) \quad \text{at} \quad r = 1 \quad \text{for} \quad (-G)Pe'/\mathscr{E} \ll 1. \tag{2.34}$$

These expressions are identical to what was found before by Foster (1999), but now the swirl velocity, which was zero in the no-rotation case is given by

$$v = \frac{2\mathscr{T}}{(Ra\,T_0')^{3/2}}\frac{\partial f}{\partial z}\left[\sqrt{2}\mathrm{e}^{\beta\xi}\cos\left(\beta\xi - \frac{\pi}{4}\right) - 1\right], \tag{2.35}$$

where $\beta \equiv (T_0')^{1/4}/\sqrt{2}$.

Once the Taylor number is as large as $O(Ra^{3/4})$, the layer structure is governed, from (2.31), by the higher-order equation

$$w_{\xi\xi\xi\xi\xi\xi} + \left(T_0' + \frac{G}{\mathscr{E}}C_0'(z)\right)w_{\xi\xi} + 4\frac{\mathscr{T}^2}{Ra^{3/2}}w_{zz} = 0 \quad \text{for} \quad \mathscr{T} = O(Ra^{3/4}). \tag{2.36}$$

The solutions to this equation are clearly non-local – unlike the previous case – and so the equation must be solved simultaneously with the outer problem.

If the Taylor number exceeds $Ra^{3/4}$, then the layer thickness is $\mathscr{T}^{-1/3}$, the equation being that of the 'Stewartson 1/3-layer' of rapidly-rotating flow theory (Stewartson 1966). Again, the solutions are non-local.

Although the buoyancy layer persists for $\mathscr{T}$ up to $O(Ra^{3/4})$, an additional layer arises exterior to the buoyancy layer for values of $\mathscr{T} \gg Ra^{1/2}$; its width is $O(Ra^{1/2}/\mathscr{T})$.

If we write $r-1=(Ra^{1/2}/\mathscr{T})\hat{r}$, then the equation in this new layer is

$$\left(T_0'+\frac{G}{\mathscr{E}}C_0'(0)\right)w_{\hat{r}\hat{r}}+4w_{zz}=0 \quad \text{for } Ra^{1/2}\ll\mathscr{T}\ll Ra^{3/4}. \tag{2.37}$$

Clearly the layer merges into the complicated, combined layer at $\mathscr{T}=O(Ra^{3/4})$, described by (2.36), and at the other extreme, for $\mathscr{T}=O(Ra^{1/2})$, the layer thickness goes to infinity, indicating a new interior structure is present at this order of $\mathscr{T}$.

3. The interfacial boundary layer

Before proceeding to the outer expansion, it is important to look closely at the structure of the boundary layer on the crystal–melt interface. Applying the usual boundary-layer approximations to equations (2.5)–(2.8), for a layer near $z=0$, we have

$$-2\mathscr{T}v+p_r=u_{zz}, \quad 2\mathscr{T}u+\frac{p_\theta}{r}=v_{zz}, \tag{3.1}$$

$$p_z=T+c, \quad T_{zz}=Ra\,T_0'w, \quad c_{zz}=\frac{GRa}{\mathscr{E}}C_0'(0)w, \tag{3.2a–c}$$

where we have not explicitly written down the nonlinear terms, taking $\mathscr{B}$ to be sufficiently small to make their neglect appropriate. The first two of these equations, utilizing continuity, can be better written in terms of the vertical velocity, the pressure and the vertical vorticity component, as

$$\nabla_h^2 p-2\mathscr{T}\zeta=-w_{zzz}, \quad -2\mathscr{T}w=\zeta_z, \quad r\zeta\equiv(rv)_r-u_\theta. \tag{3.3}$$

Eliminating ζ, w, T and c leads to a single equation for the pressure in this boundary-layer region as

$$p_{zzzzzz}+4\mathscr{T}^2p_{zz}+Ra\left(T_0'+\frac{G}{\mathscr{E}}C_0'(0)\right)\nabla_h^2p=0. \tag{3.4}$$

The non-rotating scaling is quickly recovered from this result: the boundary-layer width is $O(Ra^{-1/6})$. Clearly, that scaling is valid only for $\mathscr{T}\ll Ra^{1/3}$; this restriction is much more severe than that coming from the sidewall layer. Therefore, as Ω increases, rotation effects are felt first in this layer, long before any evidence of rotation appears in the sidewall layer. If we take the Taylor number to be of order $Ra^{1/3}$, then all terms in (3.4) are of equal magnitude. The outflow at the edge of the layer remains $O(Ra^{-1/6})$, as compared with the horizontal components.

Also instructive is the magnitude of the vertical vorticity in the layer. We now scale the vertical velocity as $w=Ra^{-1/6}\acute{w}$, and the vertical coordinate as $z=Ra^{-1/6}\acute{z}$. Then, from (3.3),

$$\zeta_{edge}=-\frac{2\mathscr{T}}{Ra^{1/3}}\int_0^\infty \acute{w}\,\mathrm{d}\acute{z}. \tag{3.5}$$

Therefore, once $\mathscr{T}$ is as large as $O(Ra^{1/3})$, the vorticity in the outer flow at the edge of the layer is the same order as the velocity components, and hence the outer flow is *not* irrotational as it is in the $\mathscr{T}\equiv 0$ case.

For $\mathscr{T}\gg Ra^{1/3}$, the layer described by (3.4) becomes double-structured, for values of $\mathscr{T}$ up to $O(Ra^{1/2})$. The inner layer is a standard Ekman layer, of width $\mathscr{T}^{-1/2}$, and

the (thicker) outer layer is described by writing $z = (\mathscr{T}/Ra^{1/2})\hat{z}$, and its equation is

$$4p_{\hat{z}\hat{z}} + \left(T_0' + \frac{G}{\mathscr{E}}C_0'(0)\right)\nabla_h^2 p = 0, \quad \text{for } Ra^{1/3} \ll \mathscr{T} \ll Ra^{1/2}. \tag{3.6}$$

For $\mathscr{T} = O(Ra^{1/2})$ and larger, this layer merges into the interior, and there is an Ekman layer only.

Since in this paper we consider only the 'thermally dominant' scenario, which implies that $Ra \gg |Ra_c|$, the coefficient of $\nabla_h^2 p$ in (3.4) and (3.6) becomes T_0' only – the $C_0'(0)$ term is much smaller and negligible to leading order.

3.1. *Other horizontal layers*

In addition to the boundary layer on the interface, there are other horizontal layers in the melt. In every case, a layer or layers exist on the upper boundary at $z = L_1$. In ways described quantitatively in § 2 and more completely in Foster (1999), that layer is required to complete the circulation pattern in the 'upper eddy' of the melt. In addition, in some of the parameter ranges explored in this paper, as in the case for $\mathscr{T} \equiv 0$ already outlined, there is the need for an adjustment layer, Region III of figure 2. Since neither of these layers has a direct bearing on the crystalline segregation, no details of either layer are given in this paper by reason of brevity.

4. The interior solutions for $\mathscr{T} = O(1)$

Before proceeding to cases for which the rotation makes a difference in the structure of the singular layers, we examine the situation for which rotation first makes a difference in the melt flow: in the interior of the melt, only. Because the inflow into the sidewall boundary layer is $O(Ra^{-1/6})$, it appears that the asymptotic series in the interior of the fluid should be, as for the non-rotating case,

$$\boldsymbol{u} = Ra^{-1}\boldsymbol{U}^{(0)} + \cdots, \quad T = T^{(0)} + \delta T^{(1)} + \cdots, \quad c = c^{(0)} + \delta c^{(1)} + \cdots, \tag{4.1}$$

$$\bar{T} = \bar{T}^{(0)} + \delta \bar{T}^{(1)} + \cdots, \tag{4.2}$$

where δ is the horizontal layer thickness, $Ra^{-1/6}$.

First, in the solid, the first-order problem is

$$\nabla^2 \bar{T}^{(0)} = 0, \qquad \bar{T}^{(0)} = 0 \quad \text{at } z = -L_2, \qquad \bar{T}_r^{(0)} = \bar{f} \quad \text{at } r = 1. \tag{4.3}$$

To this boundary-value problem must be added the joining conditions at $z = Z$, which come out of (2.14) and (2.15). Problem (4.3) clearly is unchanged throughout the parameter regimes of this problem.

Now, as to the flow in the melt, the first-order equations are

$$\nabla p^{(0)} = (T^{(0)} + c^{(0)})\boldsymbol{k}, \quad T_0' W^{(0)} = \nabla^2 T^{(0)}, \quad \nabla^2 c^{(0)} + Pe' c_z^{(0)} = 0. \tag{4.4a–c}$$

In the non-rotating analysis, it was convenient to split the solution into an azimuthally averaged and an azimuthally varying segment; that can be done here as well, but we defer that until later. The solutions to (4.4) are highly non-unique. To obtain the equations that resolve that non-uniqueness, we must proceed to higher order. At sixth order, the equations become

$$2\mathscr{T}\boldsymbol{k} \times \boldsymbol{U}^{(0)} + \nabla p^{(6)} = (T^{(6)} + c^{(6)})\boldsymbol{k} + \nabla^2 \boldsymbol{U}^{(0)}, \tag{4.5}$$

$$T_0' W^{(6)} = \nabla^2 T^{(6)}, \quad \nabla^2 c^{(6)} + Pe' c_z^{(6)} = 0, \tag{4.6}$$

provided that $GPe'/\mathscr{E}$ is sufficiently small. The vertical component of the curl of (4.5) is

$$-2\mathscr{T}\frac{\partial W^{(0)}}{\partial z} = \nabla^2\zeta^{(0)}, \quad \zeta^{(0)} = \frac{1}{r}\frac{\partial(rV^{(0)})}{\partial r} - \frac{1}{r}\frac{\partial U^{(0)}}{\partial\theta}. \tag{4.7}$$

4.1. *Azimuthally averaged component*

Splitting the solution into azimuthally averaged and azimuthally varying components, then averaging equations (4.4)–(4.7), it turns out as before (Foster 1999) that $\langle c^{(0)}\rangle \equiv 0$. Then, (4.4*a*) indicates that $\langle T^{(0)}\rangle$ is solely a function of z, and so (4.4*b*) shows that $\langle W^{(0)}\rangle$, too, depends only on z, in which case the averaged continuity equation may be simply integrated to give

$$\langle U^{(0)}\rangle = \frac{r}{2}\frac{\mathrm{d}\langle W^{(0)}\rangle}{\mathrm{d}z}. \tag{4.8}$$

Boundary condition (2.34) then permits the evaluation of $\langle W^{(0)}\rangle$, so

$$\langle W^{(0)}\rangle = -\frac{2\langle f\rangle}{T_0'}, \quad \langle U^{(0)}\rangle = r\frac{\langle f'\rangle}{T_0'}. \tag{4.9}$$

Substitution of this result into averaged (4.7) gives the equation for the averaged vorticity,

$$\nabla^2\langle\zeta^{(0)}\rangle = \frac{4\mathscr{T}}{T_0'}\langle f_1\rangle r. \tag{4.10}$$

We have seen in §§ 2.3, 3 that for $\mathscr{T} = O(1)$, $\zeta^{(0)} = 0$ at the edge of both horizontal and vertical boundary layers. If we let $\{\beta_n\}$ be the set of zeros of the Bessel function $J_0(x)$, then the solution of (4.10) may be written as a Fourier–Bessel series

$$\langle\zeta^{(0)}\rangle = \sum_{n=1}^{\infty} A_n(z)J_0(\beta_n r), \tag{4.11}$$

and

$$A_n(z) = -\frac{4\mathscr{T}\langle f_1\rangle r_n}{T_0'}\left[1 - \frac{\sinh(\beta_n z)}{\sinh(\beta_n L_1)} - \frac{\sinh(\beta_n(L_1 - z))}{\sinh(\beta_n L_1)}\right], \tag{4.12}$$

where r_n is a Fourier coefficient for r. Then, one more integral gives the variation of the averaged swirl in the interior,

$$\langle V^{(0)}\rangle = \sum_{n=1}^{\infty}\frac{A_n(z)}{\beta_n^2 r}\int_0^{\beta_n r}\xi J_0(\xi)\,\mathrm{d}\xi. \tag{4.13}$$

So, perhaps not surprisingly, the Coriolis accelerations lead to a swirl velocity in the interior even with axisymmetric heating. The remainder of the solution for this axisymmetric segment of the problem proceeds exactly as in Foster (1997). Briefly, that is as follows. Both the temperature, $\langle T^{(0)}(z)\rangle$, a solution of the equation (4.4*b*), and the solution of (4.3) in the solid vanish at $z = 0$. In that case, there is net heat flux into the interface, resulting in motion in the interfacial layer, with a speed of magnitude $Ra^{-2/3}$. The motion, and corresponding interfacial deflection, lead to solutal variations of $O(\mathscr{B}Ra^{-1/6})$.

However, though there are changes in the details of the interior melt flow, because of the presence of swirl at the interfacial layer's edge, there is no change in the

qualitative character of the solution as compared with that for no ampoule rotation because the eddy above the interface is essentially unchanged.

4.1.1. *The thermal solution*

Even though the solution for this problem is essentially already written out in Foster (1997), it is important to summarize the results here for subsequent reference. First, it turns out that $\langle c^{(0)}\rangle \equiv 0$. Then, the solution to the equation in the solid, given by (4.3), is straightforward, and – using the notation in Foster (1999) – results in

$$\langle \bar{T}^{(0)}_{rz}\rangle_{z=0} = \sum_{n=1}^{\infty} Q'''_n(0) J_1(\alpha_{0n} r), \tag{4.14}$$

$$Q'''_n(0) = \frac{2(-1)^n[\bar{T}_0(-L_2) - \bar{T}_a]}{\mathscr{K}} \sinh(\alpha_{0n} L_2) + \frac{2(-1)^n}{\mathscr{K} \sinh(\alpha_{0n} L_2)} \times \left[\frac{\sinh[\alpha_{0n}(L_2 - \bar{z}_I)]}{\alpha_{0n}} \bar{T}'_0 - [\bar{T}_0(-\bar{z}_I) - \bar{T}_a]\cosh[\alpha_{0n}(L_2 - \bar{z}_I)]\right]. \tag{4.15}$$

The quantities $\{\alpha_{0n}\}$ are the zeros of J'_0. Integration of (3.2*b*) across the boundary layer connects result (4.14), (4.15) to the boundary-layer flow, so that

$$-\mathscr{K}\langle \bar{T}^{(0)}_{rz}\rangle_{z=0} = Ra^{5/6} T'_0 \int_0^{\infty} \langle w\rangle \, \mathrm{d}\acute{z}, \tag{4.16}$$

where, as in § 3, $\acute{z} = Ra^{1/6} z$. The scale of $\langle w\rangle$ is clearly $Ra^{-5/6}$, making $\langle u\rangle$ of order $Ra^{-2/3}$. Letting $\langle u\rangle = Ra^{-2/3}\acute{u}$, the other interfacial boundary conditions in § 2.2, when combined, eventually give

$$\langle c^{(1)}_{rz}\rangle = \frac{(k-1)T'_0 + (M + kG)C'_0(0)}{T'_0 - MC'_0(0)} Pe' \langle c^{(1)}\rangle - \frac{Pe' k G C'_0(0)}{T'_0 - MC'_0(0)} \acute{u}_{\acute{z}\acute{z}\acute{z}}, \tag{4.17}$$

to be applied at $z = \acute{z} = 0$. The structure of the boundary layer allows $\acute{u}_{\acute{z}\acute{z}\acute{z}}$ to be related to the thermal gradient from (4.16). That relationship is

$$\acute{u}_{\acute{z}\acute{z}\acute{z}}|_{\acute{z}=0} = 2\mathscr{K} \sum_{n=1}^{\infty} \frac{Q'''_n(0)}{p_n} J_1(\alpha_{0n} r), \tag{4.18}$$

and $p_n \equiv (\alpha^2_{0n} T'_0)^{1/6}$. The concentration perturbation $\langle c^{(1)}\rangle$ obeys the same equation as $c^{(0)}$ in (4.4), and the solution is given by

$$\langle c^{(1)}_r\rangle = \sum_{n=1}^{\infty} R_n(z) J_1(\alpha_{0n} r), \tag{4.19}$$

where

$$R_n(0) = -\frac{2Pe' k G C'_0(0)\mathscr{K}}{T'_0 - MC'_0(0) + \Gamma\alpha^2_{0n}} \frac{Q'''_n(0)}{3p_n} \frac{\tanh(\mathscr{G}_n L_1)}{s_n \tanh(\mathscr{G}_n L_1) + \mathscr{G}_n}, \tag{4.20}$$

$$\left.\begin{aligned} s_n &\equiv \left[\frac{1}{2} + \frac{(k-1)T'_0 + (M + kG)C'_0(0) - \Gamma\alpha^2_{0n}}{T'_0 - MC'_0(0) + \Gamma\alpha^2_{0n}}\right] Pe', \\ \mathscr{G}_n &\equiv \sqrt{\frac{Pe'^2}{4} + \alpha^2_{0n}}. \end{aligned}\right\} \tag{4.21}$$

4.2. *Azimuthally varying component*

Now, according to (4.4*a*), $\tilde{T}^{(0)} = -\tilde{c}^{(0)}$, so that from (4.4*c*),

$$\nabla^2 \tilde{T}^{(0)} + Pe' \tilde{T}_z^{(0)} = 0, \qquad \tilde{T}_r^{(0)} = 0 \quad \text{at} \quad r = 1, \qquad \tilde{T}^{(0)} = 0 \quad \text{at} \quad z = L_1. \tag{4.22}$$

This equation must be solved subject to the appropriate conditions at the interface, where the solution is joined with the solution to (4.3) in $z < 0$. Supposing for the moment that has been done, the vertical velocity distribution throughout the melt is given from (4.4*b*) by

$$\tilde{W}^{(0)} = \frac{1}{T_0'} \nabla^2 \tilde{T}^{(0)}. \tag{4.23}$$

Then, using continuity and (4.7), we obtain a pair of simultaneous equations for $\tilde{U}^{(0)}$ and $\tilde{V}^{(0)}$, namely

$$\frac{1}{r} \frac{\partial (r \tilde{U}^{(0)})}{\partial r} + \frac{1}{r} \frac{\partial \tilde{V}^{(0)}}{\partial \theta} = -\frac{\partial \tilde{W}^{(0)}}{\partial z}, \tag{4.24}$$

$$\nabla^2 \tilde{\zeta}^{(0)} = -2\mathscr{T} \frac{\partial \tilde{W}^{(0)}}{\partial z}. \tag{4.25}$$

Since the properties of all of the boundary layers require that $\tilde{\zeta}^{(0)}$ vanishes at their edges, this equation may be solved, most simply in the form

$$\tilde{\zeta}^{(0)} = -\frac{2\mathscr{T}}{T_0'} \frac{\partial \tilde{T}^{(0)}}{\partial z} + \Phi, \quad \nabla^2 \Phi = 0, \quad \tilde{\zeta}^{(0)} = 0 \quad \text{on all boundaries.} \tag{4.26}$$

Equation (4.24) may then be put into a form for $\tilde{M}^{(0)} \equiv r\tilde{U}^{(0)}$, namely

$$\nabla_h^2 \tilde{M}^{(0)} = -\frac{\partial \tilde{\zeta}^{(0)}}{\partial \theta} - \frac{\partial}{\partial z} \frac{1}{r} \frac{\partial (r \tilde{W}^{(0)})}{\partial r}, \tag{4.27}$$

to be solved under boundary conditions

$$\tilde{M}^{(0)} = f \quad \text{at} \quad r = 1; \quad \tilde{M}^{(0)} = 0 \quad \text{at} \quad z = 0, L_1. \tag{4.28}$$

It looks as though the solution has changed significantly from the $\mathscr{T} \equiv 0$ case, but in fact it has not. Carefully examining the interfacial layer indicates that $\tilde{T}_z^{(0)}$ must be zero at $z = 0$, and hence the unique solution is $\tilde{T}^{(0)} \equiv 0$. Then, (4.23) indicates that $\tilde{W}^{(0)} \equiv 0$, so the flow is in horizontal planes in and out of the sidewall layers. From (4.26), $\tilde{\zeta}^{(0)} \equiv 0$ too, making that planar flow irrotational as in Foster (1999). Then, the solution of (4.27), (4.28) subject to (2.34) is

$$\tilde{U}^{(0)} - \mathrm{i}\tilde{V}^{(0)} = \frac{1}{T_0'} \sum_{m=1}^{\infty} a_m' r^{m-1} \mathrm{e}^{\mathrm{i}m\theta}. \tag{4.29}$$

Hence, the first non-zero thermal and solutal perturbations are $O(Ra^{-1/6})$, as for $\mathscr{T} \equiv 0$, and so there is no change in the segregation in the crystal at this order. So, the added swirl is not coupled to the thermal fields. The details of the analysis leading to the solutal variation at the interface are not that different from the axisymmetric case given in § 4.1.1 (Foster 1999). The single summations in (4.14), (4.20) and (4.19) become double sums, including a summation over Fourier series components in the θ-direction.

The magnitudes of the velocity vectors in the various regions of the melt are shown in the first two entries of table 1.

$\mathscr{T}$ range, axisymmetric?	Section	Region IV (u,v,w)	Region V (u,v,w)	Region VI (u,v,w)	Z
$\mathscr{T}=O(1)$, Y	4.1	$(\epsilon^{2/3},\epsilon,\epsilon^{5/6})$	$(\epsilon,\epsilon,\epsilon)$	$(\epsilon^{7/6},\epsilon,\epsilon^{7/6})$	$\mathscr{B}\epsilon^{1/6}$
$\mathscr{T}=O(1)$, N	4.2	$(\epsilon^{2/3},\epsilon,\epsilon^{5/6})$	$(\epsilon,\epsilon,\epsilon^{7/6})$	$(\epsilon^{7/6},\epsilon^{7/6},\epsilon^{7/6})$	$\mathscr{B}\epsilon^{1/6}$
$1\ll\mathscr{T}\ll\epsilon^{-1/3}$, Y	5.1	$(\epsilon^{2/3},\mathscr{T}\epsilon,\epsilon^{5/6})$	$(\epsilon,\epsilon\mathscr{T},\epsilon)$	$(\epsilon^{7/6},\mathscr{T}\epsilon,\epsilon^{7/6})$	$\mathscr{B}\epsilon^{1/6}$
$1\ll\mathscr{T}\ll\epsilon^{-1/6}$, N	5.2.1	$(\epsilon^{2/3},\mathscr{T}\epsilon,\epsilon^{5/6})$	$(\epsilon,\epsilon,\epsilon^{7/6})$	$\left(\frac{\epsilon}{\mathscr{T}},\frac{\epsilon}{\mathscr{T}},\epsilon^{7/6}\right)$	$\mathscr{B}\epsilon^{1/6}$
$\epsilon^{-1/6}\ll\mathscr{T}\ll\epsilon^{-1/3}$, N	5.2.2	$(\epsilon^{2/3},\mathscr{T}\epsilon,\epsilon^{5/6})$	$(\mathscr{T}\epsilon^{7/6},\mathscr{T}\epsilon^{7/6},\epsilon^{7/6})$	$(\mathscr{T}\epsilon^{7/6},\mathscr{T}\epsilon^{7/6},\epsilon^{7/6})$	$\mathscr{B}\epsilon^{1/6}$
$\mathscr{T}=O(\epsilon^{-1/3})$, Y	6	$(\epsilon^{2/3},\epsilon^{2/3},\epsilon^{5/6})$	$(\epsilon,\epsilon^{2/3},\epsilon)$	$(\epsilon,\epsilon^{2/3},\epsilon)$	$\mathscr{B}\epsilon^{1/6}$
$\epsilon^{-1/3}\ll\mathscr{T}\ll\epsilon^{-1/2}$, N	7	$(\epsilon,\epsilon,\frac{\epsilon}{\mathscr{T}^{1/2}})$	$(\epsilon,\epsilon,\mathscr{T}\epsilon^{3/2})$	$(\epsilon,\epsilon,\mathscr{T}\epsilon^{3/2})$	$\mathscr{B}\mathscr{T}\epsilon^{1/2}$
$\mathscr{T}=O(\epsilon^{-1/2})$, Y	8	$(\epsilon^{3/4},\epsilon^{3/4},\epsilon)$	$(\epsilon,\frac{1}{\mathscr{T}},\epsilon)$	$(\epsilon,\mathscr{T}^{-1},\epsilon)$	$\mathscr{B}$
$\mathscr{T}=O(\epsilon^{-1})$, Y	9	$\left(\frac{2}{\mathscr{T}},\frac{1}{\mathscr{T}},\frac{1}{\mathscr{T}^{3/2}}\right)$	$\left(\frac{1}{\mathscr{T}^{3/2}},\frac{1}{\mathscr{T}},\frac{1}{\mathscr{T}^{3/2}}\right)$	$\left(\frac{1}{\mathscr{T}^{3/2}},\frac{1}{\mathscr{T}},\frac{1}{\mathscr{T}^{3/2}}\right)$	$\mathscr{B}$

TABLE 1. Velocity magnitudes in Regions IV–VI of figure 2 in the various Taylor number regimes of the paper. Here, $\epsilon = Ra^{-1}$.

5. Solutions for $1 \ll \mathscr{T} \ll Ra^{1/3}$

Surprisingly, perhaps, once the Taylor number gets large, the structure of the flow field is very strongly dependent on whether or not there is azimuthal dependence of the sidewall heating. We first consider the case for which there is axisymmetry, then turn to the azimuthally varying case in the subsequent section.

The immediate reason for the restriction given in the title of this section is that, as noted in § 3, so long as the Taylor number is smaller than order $Ra^{1/3}$, there is no change in the structure of the interfacial boundary layer. We now turn first to the interior structure, which is modified by the largeness of $\mathscr{T}$.

5.1. *The interior structure for the axisymmetric case*

The sidewall inflow demands that u be $O(Ra^{-1})$, and since there can be no θ variation in the averaged swirl, continuity requires that $\langle w\rangle$ be the same order. The azimuthal component of (2.6) then forces the swirl velocity be larger than u by $O(\mathscr{T})$. Thus, we write $v = \mathscr{T}\hat{v}$. Using $\hat{\boldsymbol{u}}$ to denote the velocity vector with only the swirl rescaled, the outer expansion apparently takes the form

$$\langle\hat{\boldsymbol{u}}\rangle = \frac{1}{Ra}\langle\hat{\boldsymbol{U}}^{(0)}\rangle + \frac{1}{Ra^{7/6}}\langle\hat{\boldsymbol{U}}^{(1)}\rangle + \cdots, \tag{5.1}$$

$$\langle T\rangle = \langle T^{(0)}\rangle + \frac{1}{Ra^{1/6}}\langle T^{(1)}\rangle + \frac{\mathscr{T}^2}{Ra^{7/6}}\langle T^{(2)}\rangle + \cdots, \tag{5.2}$$

and similarly for c, except that the $O(1)$ term is absent. The second term in each series as usual is required for matching of the crystal–melt boundary layer temperature perturbations. Coriolis force then generates the third term in each series. Substitution into the equations of motion gives

$$\nabla\langle p^{(0)}\rangle = \langle T^{(0)}\rangle\boldsymbol{k}, \quad T_0'\langle\hat{W}^{(0)}\rangle = \nabla^2\langle T^{(0)}\rangle. \tag{5.3a,b}$$

Clearly, $\langle\hat{W}^{(0)}\rangle$ and hence $\langle T^{(0)}\rangle$ are functions of z alone. Thus, continuity can be

solved trivially to give

$$\langle \hat{W}^{(0)} \rangle = -2\frac{\langle f(z) \rangle}{T_0'}, \quad \langle \hat{U}^{(0)} \rangle = r\frac{\langle f' \rangle}{T_0'}. \tag{5.4}$$

Then, from (5.3*b*),

$$\frac{\mathrm{d}^2\langle T^{(0)} \rangle}{\mathrm{d}z^2} = -2\langle f \rangle, \tag{5.5}$$

and the azimuthal momentum equation becomes

$$\mathscr{D}^2\langle \hat{V}^{(0)} \rangle = 2r\frac{\langle f' \rangle}{T_0'}, \quad \mathscr{D}^2 \equiv \nabla^2 - \frac{1}{r^2}. \tag{5.6}$$

Terms of subsequent orders can be determined from equations further down the hierarchy without difficulty, in spite of the complication that the terms with superscripts 2 and 3 interchange orders if $\mathscr{T} \gg Ra^{1/4}$.

Equation (5.6) for $\langle \hat{V}^{(0)} \rangle$ may be easily solved, utilizing $\langle f \rangle$ from the thermal boundary condition. The solution is

$$\langle \hat{V}^{(0)} \rangle = \frac{r^3 - r}{4} H(z - z_I) + \sum_{n=1}^{\infty} A_n(z) J_1(\alpha_{0n} r), \tag{5.7}$$

$$A_n = -C_n \sinh(\alpha_{0n}(L_1 - z)) \cosh(\alpha_{0n} z_I), \quad z > z_I, \tag{5.8}$$

$$A_n = C_n \cosh(\alpha_{0n}(L_1 - z_I)) \sinh(\alpha_{0n} z), \quad z < z_I, \tag{5.9}$$

and the coefficient is given by

$$C_n = \frac{1}{\alpha_{0n}[J_0(\alpha_{0n})]^2 \sinh(\alpha_{0n} L_1)} \int_0^1 (2r^3 - 2r) J_0(\alpha_{0n} r)\, \mathrm{d}r. \tag{5.10}$$

As in the case of the axisymmetric problem analysed in a previous paper (Foster 1997) and reiterated briefly in § 4, the solution of the $\langle T^{(0)} \rangle$ problem, with $\langle T^{(0)} \rangle$ a function of z only, can be found without surface deflection. So, problem (5.3*b*) is to be solved subject to $\langle T^{(0)} \rangle = 0$ at $z = 0$, and the solution for $\langle \bar{T}^{(0)} \rangle$ has properties already given in (4.14), (4.15). That leaves a flux mis-match at $z = 0$, leading again to $O(Ra^{-2/3})$ radial velocity in the interfacial layer, and solutal variation at the interface of $O(\mathscr{B}Ra^{-1/6})$. All of the thermal and solutal fields, and the interfacial layer are exactly as reiterated in § 4.1.1 for $\mathscr{T} = O(1)$. Thus, once again, the added Coriolis-induced swirl does not couple to the temperature distribution in the material.

Table 1 exhibits velocity magnitudes in Regions IV–VI for this range of $\mathscr{T}$.

5.2. *The interior structure for the non-axisymmetric case*

The outer expansions exhibited at the beginning of § 4 must now be modified in a way that is different from the modification above for the axisymmetric case. Indeed, we find differences depending on the magnitude of $\mathscr{T}$ relative to $Ra^{-1/6}$, so we consider two cases separately below. As will be shown, the differences are in the interior flow structure, but the separation at the interfacial boundary is unchanged from the $\mathscr{T} = O(1)$ regime.

5.2.1. $1 \ll \mathscr{T} \ll Ra^{1/6}$

The inflow demands of the sidewall layer are unchanged, so the first term in the velocity expansion remains $O(Ra^{-1})$, but the next terms in the series *are* changed, so

we write for the azimuthally varying component,

$$\tilde{\boldsymbol{u}} = \frac{1}{Ra}\tilde{\boldsymbol{U}}^{(0)} + \frac{1}{\mathscr{T}Ra}\tilde{\boldsymbol{U}}^{(1)} + \frac{1}{Ra^{7/6}}\tilde{\boldsymbol{U}}^{(2)} + \cdots, \tag{5.11}$$

$$(\tilde{T}, \tilde{c}) = \frac{1}{\mathscr{T}}(\tilde{T}^{(0)}, \tilde{c}^{(0)}) + \frac{1}{Ra^{1/6}}(\tilde{T}^{(1)}, \tilde{c}^{(1)}) + \cdots. \tag{5.12}$$

Substitution into the Navier–Stokes equations, (2.6), for sufficiently small $\mathscr{B}$, with some manipulation gives $\tilde{W}^{(0)} \equiv 0$ and the following equations valid for $j = 0, 1$:

$$\tilde{T}^{(j)} + \tilde{c}^{(j)} = 0, \tag{5.13}$$

$$T_0'\tilde{W}^{(j+1)} = \nabla^2\tilde{T}^{(j)}, \tag{5.14}$$

$$-2\frac{\partial \tilde{W}^{(j+1)}}{\partial z} = \nabla^2\tilde{\zeta}^{(j)}, \tag{5.15}$$

where ζ is, as before, the vertical component of vorticity. The concentration perturbation, $\tilde{c}^{(j)}$, satisfies the equation

$$\nabla^2\tilde{c}^{(j)} + Pe'\tilde{c}_z^{(j)} = 0, \quad j = 0, 1. \tag{5.16}$$

The boundary layer at the crystal–melt interface discussed in § 3 cannot handle the large heat flux from the $\tilde{T}^{(0)}$ field, hence $\tilde{T}_z^{(0)} = 0$ at $z = 0$, which implies then that

$$\tilde{W}^{(1)} = \tilde{T}^{(0)} = \tilde{c}^{(0)} \equiv 0. \tag{5.17}$$

Now, this result implies that $\tilde{\zeta}^{(0)} \equiv 0$, so the irrotational horizontal flow given in (4.29) is still valid.

Since $\tilde{T}^{(1)}$ also satisfies (5.16), the structure and solution of the interfacial layer is unchanged from $\mathscr{T} \equiv 0$. In contrast with (4.29), the new term in the velocity series, $(Ra\mathscr{T})^{-1}$, is again in horizontal layers, but rotational, since the vorticity is a solution of the equation

$$\nabla^2\tilde{\zeta}^{(1)} = \frac{2Pe'}{T_0'}\tilde{T}_{zz}^{(1)}. \tag{5.18}$$

Note that this motion is spread throughout Regions V and VI of figure 2, so azimuthally varying flow is induced nearer the interface than in the previous parameter range. This 'smearing-out' of the swirling flow, $\tilde{\boldsymbol{U}}^{(1)}$, is in contrast to the $\tilde{\boldsymbol{U}}^{(0)}$ flow, which is discontinuous at $z = z_I$ and must be smoothed with a transitional layer. So, though there is an indication that the upper-eddy dynamics will influence what happens near the interface at perhaps larger $\mathscr{T}$ values, it has not happened yet: the balances in the interfacial layer are unchanged, and hence the radial segregation remains $O(\mathscr{B}Ra^{-1/6})$.

5.2.2. $Ra^{1/6} \ll \mathscr{T} \ll Ra^{1/3}$

At this level for $\mathscr{T}$, the Coriolis forces generate still larger swirling flows, hence the outer expansion takes the modified form

$$\tilde{\boldsymbol{u}} = \frac{\mathscr{T}}{Ra^{7/6}}\tilde{\boldsymbol{U}}^{(0)} + \frac{1}{Ra}\tilde{\boldsymbol{U}}^{(1)} + \frac{1}{Ra^{7/6}}\tilde{\boldsymbol{U}}^{(2)} + \cdots, \tag{5.19}$$

$$(\tilde{T}, \tilde{c}) = \frac{1}{Ra^{1/6}}(\tilde{T}^{(0)}, \tilde{c}^{(0)}) + \frac{1}{\mathscr{T}}(\tilde{T}^{(1)}, \tilde{c}^{(1)}) + \cdots. \tag{5.20}$$

As before, we find immediately that

$$\tilde{W}^{(0)} = \tilde{W}^{(1)} = 0. \tag{5.21}$$

Leaving out some details, which are very like those above in § 5.2.1, the important equation pair is

$$-2\frac{\partial \tilde{W}^{(2)}}{\partial z} = \nabla^2 \tilde{\zeta}^{(0)}, \tag{5.22}$$

$$T_0' \tilde{W}^{(2)} = \nabla^2 \tilde{T}^{(0)}. \tag{5.23}$$

Now, $\tilde{T}^{(0)}$ obeys equation (4.22), and the entire analysis of the thermal field is as described in that section, that is, $\tilde{T}^{(0)}$ is wholly determined by $\bar{T}^{(0)}$ and the crystal–melt boundary layer. Therefore, $\tilde{W}^{(2)}$ may then be written down from (5.23), and then the vorticity, $\tilde{\zeta}^{(0)}$, determined by (5.22). There has been a significant change here, in that the horizontal motion is now rotational, and spread throughout the melt – so that the isolation of the 'upper' and 'lower eddies' so familiar to workers on Bridgman solidification has begun to end. The horizontal velocity components in the interfacial layer are $O(Ra^{-2/3})$. The new larger outer horizontal velocity components, $O(Ra^{-7/6}\mathscr{T})$, while larger than the inflow-driven Ra^{-1}, are nonetheless still too small to affect the fundamental balances in the interfacial layer, in which mis-matched thermal flux generates non-zero $\tilde{T}^{(0)}$ in Regions V and VI. We can anticipate that once these induced flows become sufficiently strong, there is an opportunity for the basic balances in the layer to be altered, and hence segregation to be altered.

Again, velocity magnitudes in Regions IV–VI of figure 2 are summarized in table 1.

6. Axisymmetric solution for $\mathscr{T} = O(Ra^{1/3})$

In this section, we write $\mathscr{T} = \tau/\eta$, $\eta \equiv Ra^{-1/3}$, and proceed in a fashion like that above. The non-axisymmetric problem in this parameter range is not pursued here, so without ambiguity we suspend the use of the $\langle \quad \rangle$ notation in this section.

6.1. *Outer expansion*

The outer expansion proceeds as follows:

$$(u, w) = \eta^3(U^{(0)}, W^{(0)}) + \eta^{7/2}(U^{(b)}, W^{(b)}) + \eta^4(U^{(1)}, W^{(1)}) + \eta^5(U^{(2)}, W^{(2)}) + \cdots, \tag{6.1}$$

$$v = \tau\eta^2 V^{(0)} + \eta^{5/2} V^{(b)} + \tau\eta^3 V^{(1)} + \tau\eta^4 V^{(2)} + \cdots, \tag{6.2}$$

$$(T, c) = (T^{(0)}, 0) + \eta^{1/2}(T^{(b)}, c^{(b)}) + \eta(T^{(1)}, c^{(1)}) + \eta^2(T^{(2)}, c^{(2)}) + \cdots. \tag{6.3}$$

The terms with superscript (b) have been added to account for effects due to the interfacial layer. Substitution into the equations of motion gives, for the second and third terms in the temperature series, identical equations, hence

$$\nabla P^{(s)} = (T^{(s)} + c^{(s)})\boldsymbol{k}, \quad T_0' W^{(s)} = \nabla^2 T^{(s)}, \quad s = 0, b, \tag{6.4}$$

and, for $n = 1, 2$,

$$-2\tau^2 V^{(n-1)} + P_r^{(n)} = 0, \quad P_z^{(n)} = T^{(n)} + c^{(n)}, \quad 2U^{(n-1)} = \mathscr{D}^2 V^{(n-1)}. \tag{6.5}$$

The next terms then lead to

$$-2\tau^2 V_z^{(2)} = \mathscr{D}^2(U_z^{(0)} - W_r^{(0)}) - T_r^{(3)} - c_r^{(3)}, \tag{6.6}$$

$$2U^{(2)} = \mathscr{D}^2 V^{(2)}. \tag{6.7}$$

The $T^{(0)}$ solution is identical to that found previously by Foster (1997) and the same as that for the $\mathscr{T} \ll \eta^{-1}$ case discussed in § 5.1, and the leading-order velocity components are given here too by (5.4) and, apparently, also (5.7). The leading-order swirl is then the solution of the equation

$$\mathscr{D}^2 V^{(0)} = 2r \frac{\langle f' \rangle}{T_0'}. \tag{6.8}$$

The sidewall layer structure is such that $V^{(0)} = 0$ there, but the boundary conditions at $z = 0, L_1$ are yet to be determined.

6.2. *Interfacial boundary layer*

The boundary layer analysed in § 3 is described by solutions to (3.4), which may be constructed in the usual fashion, writing u in a form that guarantees that it vanishes on the sidewall. Hence, for this axisymmetric case,

$$u = \mathscr{F} \sum_{n=1}^{\infty} R_n(\acute{z}) J_1(\alpha_{0n} r), \tag{6.9}$$

where the boundary-layer coordinate, $\acute{z} \equiv z/\eta^{1/2}$ has been introduced. The quantity $\mathscr{F}$ is an as yet unknown gauge function. Then, R_n satisfies the ordinary differential equation

$$R_n^{(\mathrm{vi})} + 4\tau^2 R_n'' - T_0' \alpha_{0n}^2 R_n = 0. \tag{6.10}$$

The solution takes the form

$$R_n = c_n \mathrm{e}^{-\lambda_n \acute{z}} + d_n \mathrm{e}^{-\mu_n \acute{z}} + d_n^* \mathrm{e}^{-\mu_n^* \acute{z}}, \tag{6.11}$$

where the asterisk denotes complex conjugate. It is easily shown that the solutions to (6.10) consist of one decaying real exponential, and two decaying oscillatory exponentials, hence the form of (6.11). As in Foster (1997), the temperature perturbation in this layer is $O(\eta^{1/2})$, so the equations of § 3 indicate that w is $O(\eta^{5/2})$, hence $u = O(\eta^2)$ ($\mathscr{F} = \eta^2$), an order smaller than the first term in the outer expansion, so indeed $u \to 0$ at the layer's edge, as already implemented in (6.11). Thus, we write formally

$$T = T^{(0)}(r, 0) + \eta^{1/2} \acute{T}, \quad c = \eta^{1/2} \acute{c}, \quad w = \eta^{5/2} \acute{w}, \quad (u, v) = \eta^2 (\acute{u}, \acute{v}). \tag{6.12}$$

The velocity boundary conditions at the wall are no slip, as usual. At the edge, we require that the vertical velocity component vanish, hence there are two conditions on R_n:

$$R_n(0) = 0, \quad \int_0^{\infty} R_n(\acute{z})\, \mathrm{d}\acute{z} = 0. \tag{6.13}$$

The third condition is the one that couples this interfacial layer to the flow away from the layer, and particularly to the sidewalls, and is obtained as before by integrating the thermal equation across the layer and using the joining condition on the thermal gradient,

$$T_z^{(0)}|_{z=0+} - \mathscr{K} \bar{T}_z^{(0)}|_{z=0-} = T_0' \sum_{n=1}^{\infty} J_0(\alpha_{0n} r) \int_0^{\infty} \acute{z} R_n(\acute{z})\, \mathrm{d}\acute{z}. \tag{6.14}$$

The quantities on the left-hand side of this equation are known, so R_n is now completely determined, and the solution may be used in the application of the other boundary conditions at the crystal–melt interface.

Interestingly, integration of the swirl equation indicates the presence of a non-zero swirl at the layer's edge,

$$\acute{v}_{\text{edge}} = -2\tau\eta^2 \int_0^\infty \acute{z}\acute{u}\,\mathrm{d}\acute{z},$$

$$\Longrightarrow \quad V^{(0)}|_{z=0} = -2\sum_{n=1}^{\infty} J_1(\alpha_{0n} r) \int_0^\infty \acute{z} R_n(\acute{z})\,\mathrm{d}\acute{z}. \tag{6.15}$$

There is a similar expression for $V^{(0)}$ at $z = L_1$, not written down here for brevity.

Before proceeding to the completion of this axisymmetric solution, we need more details of the boundary-layer solution. The root λ_n in (6.11) is the positive, real solution of

$$\lambda_n^6 + 4\tau^2\lambda_n^2 - \alpha_{0n}^2 T_0' = 0. \tag{6.16}$$

The root μ_n can be written as $\mu = |\mu_n| \exp(\mathrm{i}\psi_n)$, and it is easily shown that $|\mu_n| = X_n^{1/4}$, where X_n is the positive real root of

$$X_n^3 - 4\tau^2 X_n^2 - (\alpha_{0n}^2 T_0')^2 = 0, \tag{6.17}$$

and

$$\cos(2\psi_n) = -\frac{\alpha_{0n}^2 T_0'}{2|\mu_n|^6}. \tag{6.18}$$

The angle ψ_n can be shown to vary from $\pi/3$ at $\tau = 0$ to $\pi/4$ for $\tau \to \infty$. Applying conditions (6.13) to the solution (6.11) leads to a relation between c_n and d_n, namely

$$d_n = \frac{\mathrm{i}c_n}{2} \frac{\lambda_n \mathrm{e}^{\mathrm{i}\psi_n} - |\mu_n|}{\lambda_n \sin\psi_n}. \tag{6.19}$$

The integral in (6.14) can be worked out since it comes into the solution later. It is

$$\int_0^\infty \acute{z} R_n(\acute{z})\,\mathrm{d}\acute{z} = \frac{c_n}{\lambda_n^2}\left[1 - 2\frac{\lambda_n}{|\mu_n|}\cos\psi_n + \frac{\lambda_n^2}{|\mu_n|^2}\right]. \tag{6.20}$$

6.3. *The complete solution*

Through equation (6.14), the flow in the boundary layer is completely determined. Since $T^{(0)} = T^{(0)}(z)$, taking the r-derivative of (6.14) indicates that the temperature distribution in the solid, given by $\overline{T}^{(0)}$, is solely responsible for driving the boundary-layer flow. The outer solution in general takes the form

$$\overline{T}_r^{(0)} = r\bar{f}(z) + \frac{\partial^2}{\partial z^2}\sum_{n=1}^{\infty} Q_n(z) J_1(\alpha_{0n} r), \tag{6.21}$$

and results have been given already in (4.14), (4.15). Then, using (6.14) and (6.20), the boundary-layer flow is fully determined, with

$$c_n = \frac{\mathscr{K}\lambda_n^2|\mu_n|^2}{\alpha_{0n} T_0'[\lambda_n^2 - 2\lambda_n|\mu_n|\cos\psi_n + |\mu_n|^2]} Q_n'''(0). \tag{6.22}$$

Turning now to other interfacial boundary conditions, and noting that c does not

change to leading order across the layer, (2.14) and (2.16) become

$$(T_0' - MC_0'(0))h + \acute{T} = \frac{M}{G}c^{(b)}\bigg|_{z=0} + \Gamma r^{-1}(rh_r)_r, \tag{6.23}$$

$$[c_z^{(b)} - (k-1)Pe'c^{(b)}]_{z=0} = kGC_0'(0)Pe'h, \tag{6.24}$$

where the interfacial deflection is given by $Z = \mathscr{B}Ra^{-1/6}h(r)$. Eliminating h between these two conditions,

$$(T_0' - MC_0'(0) - \Gamma\mathscr{L}^2)(c_{rz}^{(b)} - (k-1)Pe'c_r^{(b)}) = kGC_0'(0)Pe'\left(\frac{M}{G}c_r^{(b)} - \acute{T}_r\right)$$
$$\text{at } z = \acute{z} = 0, \tag{6.25}$$

where

$$\mathscr{L}^2F \equiv \frac{\partial}{\partial r}\left(\frac{1}{r}\frac{\partial(rF)}{\partial r}\right). \tag{6.26}$$

From the boundary-layer solution for $\acute{T}$, this may be rewritten as

$$(T_0' - MC_0'(0) - \Gamma\mathscr{L}^2)(c_{rz}^{(b)} - (k-1)Pe'c_r^{(b)}) - kGC_0'(0)Pe'\left(1 + \frac{M}{G}\right)c_r^{(b)}$$
$$= -kGC_0'(0)Pe'\acute{u}_{\acute{z}\acute{z}\acute{z}}|_{\acute{z}=0} \quad \text{at } z = 0. \tag{6.27}$$

Using solution (6.11) and the properties of the solution, namely the evaluation of c_n given in (6.22), the quantity on the right-hand side of (6.27) is

$$\acute{u}_{\acute{z}\acute{z}\acute{z}}\big|_{\acute{z}=0} = \sum_{n=1}^{\infty} S_nQ_n'''(0)J_1(\alpha_{0n}r), \tag{6.28}$$

where

$$S_n = \frac{[\lambda_n^4 - 4\lambda_n|\mu_n|^3\cos\psi_n\cos(2\psi_n) + |\mu_n|^4(2\cos(2\psi_n) + 1)]\mathscr{K}\lambda_n|\mu_n|^2}{\alpha_{0n}T_0'[\lambda_n^2 - 2\lambda_n|\mu_n|\cos\psi_n + |\mu_n|^2]}. \tag{6.29}$$

To complete the solution, as before we solve the equation for the solutal concentration,

$$\mathscr{D}^2c_r^{(b)} + Pe'c_{rz}^{(b)} = 0 \tag{6.30}$$

with

$$c_r^{(b)} = \sum_{n=1}^{\infty}\mathscr{C}_n(z)J_1(\alpha_{0n}r) \tag{6.31}$$

under condition (6.27). That process leads to

$$\mathscr{C}_n = g_n\mathrm{e}^{-Pe'z/2}\sinh(\mathscr{G}_n(L_1 - z)), \tag{6.32}$$

where

$$\mathscr{G}_n \equiv \sqrt{\frac{Pe'^2}{4} + \alpha_{0n}^2}, \quad g_n = \frac{kGC_0'(0)Pe'S_n}{D_n}Q_n'''(0), \tag{6.33}$$

and

$$D_n = \left[(k - \tfrac{1}{2})T_0' - \tfrac{1}{2}\Gamma\alpha_{0n}^2 + C_0'(0)(kG + \tfrac{1}{2}M)\right]Pe'\sinh(\mathscr{G}_nL_1)$$
$$+[T_0' - MC_0'(0) + \Gamma\alpha_{0n}^2]\mathscr{G}_n\cosh(\mathscr{G}_nL_1). \tag{6.34}$$

Optimization for long ampoules is precisely as for the non-rotating case: choose parameters to make $\mathscr{C}_1 = 0$, which can be done only by making $Q_1'''(0) = 0$. All that has changed here is the multiplier on $Q_n'''(0)$, the scale of c_r is still what it is for axisymmetric cases at $\mathscr{T} = 0$, namely $O(\mathscr{B}Ra^{-1/6})$.

Though we have set up the problem to be solved for $V^{(0)}$, we have not written down the solution since the thermal/solutal fields are decoupled from $V^{(0)}$.

6.3.1. *Behaviour of S_n with τ*

From (6.33), all effects of Taylor number variation in this parameter range are buried in the quantity S_n given in (6.29). It is important to note how this parameter varies with Taylor number. For small scaled Taylor number ($\tau \to 0$), $|\mu_n|, \lambda_n \to (\alpha_{0n}^2 T_0')^{1/6}$ and $\psi_n \to \pi/3$, as noted above. Therefore,

$$S_n \to \frac{\alpha_{0n}\mathscr{K}}{3(\alpha_{0n}^2 T_0')^{1/6}} \quad \text{as } \tau \to 0. \tag{6.35}$$

This result of course recovers previously obtained $\mathscr{T} \equiv 0$ results (Foster 1997). However, inspection of (6.16)–(6.18) indicates that for $\tau \to \infty$, $|\mu_n| \sim (2\tau)^{1/2}$, so that $\psi_n \to \pi/4$. In addition, $\lambda_n \to (\alpha_{0n}^2 T_0'/(4\tau^2))^{1/2}$, and therefore

$$S_n \sim \frac{\mathscr{K}}{2\sqrt{T_0'}}\tau \quad \text{as } \tau \to \infty. \tag{6.36}$$

The growth of S_n with τ at large τ gives c_r of order $\mathscr{B}\mathscr{T}/Ra^{1/2}$, suggesting that, for $\mathscr{T} = O(Ra^{1/2})$ discussed in § 8, the interfacial deflection and radial variation in c increase to $O(\mathscr{B})$. That does, in fact, turn out to be the case!

Finally, large-n modes seem least affected by finite values of τ. It is easy to show that, for $\tau = O(1)$, the behaviour of S_n for $n \to \infty$ is precisely that given by (6.35) for $\tau = 0$. The limiting form at large τ given in (6.36) is valid only for modes for which $\tau \gg (\alpha_{0n}^2 T_0')^{1/6}$; then, for $\tau \ll (\alpha_{0n}^2 T_0')^{1/6}$, the approximation (6.35) is valid. In the intermediate range, solution of the full equations (6.16)–(6.18) is required for large n.

Velocity scales for Regions IV–VI are again summarized in table 1.

7. Solutions for $Ra^{1/3} \ll \mathscr{T} \ll Ra^{1/2}$

In this parameter range, we explore the azimuthally varying segment of the flow only; the averaged portion is not unlike what we detail below in § 8. Further, there is a hint of the transition from $O(Ra^{1/3})$ to $O(Ra^{1/2})$ in § 6.3.1 for the axisymmetric case. As discussed briefly in § 3, in particular in (3.6), the interfacial boundary layer splits into a velocity layer – an Ekman layer, in fact – of width $\mathscr{T}^{-1/2}$, and a thicker thermal layer, with thickness $O(\mathscr{T}/Ra^{1/2})$. It is this splitting of the layer that leads to an increasing order in the segregation in this range.

7.1. *Outer expansion*

The outer expansion has a somewhat more complicated structure here, and proceeds as

$$\tilde{\boldsymbol{u}} = \frac{1}{Ra}\tilde{\boldsymbol{U}}^{(0)} + \frac{1}{Ra\mathscr{T}}\tilde{\boldsymbol{U}}^{(1)} + \frac{\mathscr{T}}{Ra^{3/2}}\tilde{\boldsymbol{U}}^{(2)} + \cdots, \tag{7.1}$$

$$\begin{pmatrix} \tilde{T} \\ \tilde{c} \end{pmatrix} = \frac{\mathscr{T}}{Ra^{1/2}}\begin{pmatrix} \tilde{T}^{(0)} \\ \tilde{c}^{(0)} \end{pmatrix} + \frac{\mathscr{T}}{Ra}\begin{pmatrix} \tilde{T}^{(1)} \\ \tilde{c}^{(1)} \end{pmatrix} + \frac{\mathscr{T}^2}{Ra}\begin{pmatrix} \tilde{T}^{(2)} \\ \tilde{c}^{(2)} \end{pmatrix} + \cdots. \tag{7.2}$$

Substitution into the equations of motion leads to

$$\tilde{T}^{(0)} + \tilde{c}^{(0)} = 0, \quad \nabla^2 \tilde{c}^{(0)} + Pe' \tilde{c}_z^{(0)} = 0. \tag{7.3}$$

Then, to next order,

$$-2\tilde{V}^{(0)} + \tilde{P}_r^{(1)} = 0, \quad 2\tilde{U}^{(0)} + r^{-1}\tilde{P}_\theta^{(1)} = 0, \quad \tilde{P}_z^{(1)} = \tilde{T}^{(1)} + \tilde{c}^{(1)}, \quad \tilde{W}^{(0)} = 0. \tag{7.4}$$

At still the next level it is convenient to put it into the form

$$\tilde{W}^{(1)} = 0, \quad \nabla^2 \tilde{\zeta}^{(0)} = 0. \tag{7.5}$$

Finally, to next order,

$$T_0' \tilde{W}^{(2)} = \nabla^2 \tilde{T}^{(0)}. \tag{7.6}$$

The sidewall layers yield the condition

$$\tilde{\zeta}^{(0)} = 0 \quad \text{at} \quad r = 1. \tag{7.7}$$

7.2. *The Ekman layers*

The thinner layer on the interface is an Ekman layer; the layer on $z = L_1^-$ is also an Ekman layer. Details are not given here, but what is very well known is that there is an outflow at the layer edge, so that there is a compatibility required of the outer-flow velocity components at the boundaries. (See Greenspan 1964, for example.) Hence,

$$w = \pm \frac{1}{2\mathscr{T}^{1/2}} \zeta \quad \text{at} \quad z = 0, L_1. \tag{7.8}$$

Since it is easy to verify that no vertical velocity component of $O(Ra^{-1}\mathscr{T}^{-1/2})$ is possible, we conclude that

$$\tilde{\zeta}^{(0)} = 0 \quad \text{at} \quad z = 0, L_1. \tag{7.9}$$

Therefore, the solution of the problem for $\tilde{\zeta}^{(0)}$, (7.5), is

$$\tilde{\zeta}^{(0)} \equiv 0. \tag{7.10}$$

Thus, the solution for the leading-order flow in the melt is once again given by (4.29).

7.3. *The thermal layer*

The thermal variations do not occur in the Ekman layer, but across a layer described by (3.6). The equations may be put into the somewhat more convenient form

$$\nabla_h^2 T + \frac{4\mathscr{T}^2}{Ra\, T_0'} T_{\hat{z}\hat{z}} = -\nabla^2 \tilde{c}^{(0)}\Big|_{z=0}, \tag{7.11}$$

$$T_0' w = \frac{1}{\mathscr{T}^2} T_{\hat{z}\hat{z}}, \tag{7.12}$$

where the scaling $z = (\mathscr{T}/Ra^{1/2})\hat{z}$ has been used. Writing $T = (\mathscr{T}/Ra^{1/2})\hat{\hat{T}}$ in the layer, clearly $w = (Ra^{-1/2}\mathscr{T}^{-1})\hat{\hat{w}}$. The solution for the temperature utilizing boundary condition (2.15) is, then, given by

$$\hat{\hat{T}} = \mathrm{Re}\left[\sum_{m=1}^{\infty}\sum_{n=1}^{\infty} A_{mn}(\hat{z}) e^{im\theta} J_m(\alpha_{mn} r)\right] - \tilde{c}^{(0)}|_{z=0}, \tag{7.13}$$

where

$$A_{mn} = \mathscr{K}\frac{Q'''_{mn}(0)}{b_{mn}}\mathrm{e}^{-b_{mn}\hat{z}}, \quad b_{mn} \equiv \left(\frac{\alpha_{mn}^2 Ra\, T_0'}{4\mathscr{T}^2}\right)^{1/2}, \tag{7.14}$$

and α_{mn} is the nth zero of $J'_m(x)$ as before. The coefficients $\{Q_{mn}(z)\}$ are related to the solutions of the $\tilde{\bar{T}}^{(0)}$ problem in $z < 0$, that is,

$$\tilde{\bar{T}}^{(0)} = \mathrm{Re}\left[\sum_{m=1}^{\infty}\mathrm{e}^{\mathrm{i}m\theta}\left(\frac{r^m\bar{a}_m(z)}{m} + \frac{\partial^2}{\partial z^2}\sum_{n=1}^{\infty}Q_{mn}(z)J_m(\alpha_{mn}r)\right)\right], \tag{7.15}$$

and

$$Q'''_{mn}(0) = \frac{\chi_{mn}\alpha_{mn}^3}{\sinh(\alpha_{mn}L_2)}\left[\bar{a}_m(-L_2) - \bar{a}_m(-\bar{z}_I)\cosh(\alpha_{mn}(L_2 - \bar{z}_I)) + \frac{\bar{a}'_m}{\alpha_{mn}}\sinh(\alpha_{mn}(L_2 - \bar{z}_I))\right], \tag{7.16}$$

and

$$\chi_{mn} \equiv -\frac{2J_{m+1}(\alpha_{mn})}{m(\alpha_{mn}^2 - m^2)\alpha_{mn}[J_m(\alpha_{mn})]^2}. \tag{7.17}$$

Recall that $\{\bar{a}_m\}$ are the Fourier series coefficients of the thermal boundary condition, given in (2.23). Using a substitution like (6.31), we write

$$\tilde{c}^{(0)} = \mathrm{Re}\left[\sum_{m=1}^{\infty}\mathrm{e}^{\mathrm{i}m\theta}\sum_{n=1}^{\infty}\mathscr{C}_{mn}(z)J_m(\alpha_{mn}r)\right], \tag{7.18}$$

and we obtain the solution to the solute equation in a form similar to (6.32):

$$\mathscr{C}_{mn} = \ell_{mn}\mathrm{e}^{-Pe'z/2}\sinh(v_{mn}(L_1 - z)), \qquad v_{mn} = \sqrt{\frac{Pe'^2}{4} + \alpha_{mn}^2}. \tag{7.19}$$

Writing the interfacial deflection as $\tilde{Z} = \mathscr{T}Ra^{-1/2}h(r)$, boundary conditions (2.14), (2.15) and (2.16) may be combined to give a single condition, on $\tilde{c}^{(0)}$, namely

$$(T_0' - MC_0'(0) + \Gamma\nabla_h^2)(\tilde{c}_z^{(0)} - (k-1)\tilde{c}^{(0)}) = kGC_0'(0)Pe'\left[\left(1 + \frac{M}{G}\right)\tilde{c}^{(0)} - \hat{\tilde{T}}|_{\hat{z}=0}\right] \quad \text{at } z = 0. \tag{7.20}$$

Substitution of (7.19) into (7.20) leads to the result

$$\ell_{mn} = kGPe'C_0'(0)\frac{\mathscr{K}Q'''_{mn}(0)}{\alpha_{mn}D_{mn}}\left(\frac{\mathscr{T}^2}{Ra\,T_0'}\right)^{1/2}, \tag{7.21}$$

$$D_{mn} = Pe'\left[(k - \tfrac{1}{2})(T_0' + \Gamma\alpha_{mn}^2) + (kG + \tfrac{1}{2}M)C_0'(0)\right]\sinh(v_{mn}L_1) + v_{mn}\cosh(v_{mn}L_1). \tag{7.22}$$

Again, as in the previous section, it is clear that as $\mathscr{T}$ becomes $O(Ra^{1/2})$, the solutal variations increase to $O(\mathscr{B})$.

Since $\mathscr{C}_{mn}$ is proportional to $Q'''_{mn}(0)$, optimization is precisely the same as for the $\mathscr{T} \equiv 0$ azimuthally varying case: require $Q'''_{11}(0) = 0$ (Foster 1999).

8. Axisymmetric solutions for $\mathscr{T} = O(Ra^{1/2})$

There is a significant change in axisymmetric flow structure when the Taylor number gets to this level, because the Coriolis force is now large enough to alter the $O(1)$ thermal perturbation, and making the meridional flow structure much more complicated – the dependence of the leading-order term in the T series on z alone disappears. We proceed first to the outer expansion, then to the boundary-layer structure. In this section, as in an earlier one, since there is no ambiguity, we do not use the $\langle\ \ \rangle$ notation.

8.1. *Outer expansion*

Away from any boundary layers, because of the inflow requirements at the sidewall, we write

$$(u, w) = Ra^{-1}(U^{(0)}, W^{(0)}) + Ra^{-5/4}(U^{(1)}, W^{(1)}) + \cdots, \tag{8.1}$$

$$v = \mathscr{T}^{-1}V^{(0)} + Ra^{-3/4}V^{(1)} + \cdots, \tag{8.2}$$

$$T = T^{(0)} + Ra^{-1/4}T^{(1)} + \cdots, \qquad c = c^{(0)} + Ra^{-1/4}c^{(1)} + \cdots. \tag{8.3}$$

The resulting equations are

$$\nabla \cdot \boldsymbol{U}^{(0)} = 0, \quad -2V^{(0)} + P_r^{(0)} = 0, \quad 2\frac{\mathscr{T}^2}{Ra}U^{(0)} = \mathscr{D}^2 V^{(0)}, \tag{8.4}$$

$$P_z^{(0)} = T^{(0)} + c^{(0)}, \quad T_0' W^{(0)} = \nabla^2 T^{(0)}, \quad \nabla^2 c^{(0)} + Pe' c_z^{(0)} = 0. \tag{8.5a–c}$$

Utilizing the thermal and azimuthal equations, it is possible to obtain a relatively simple relation between the two meridional components:

$$\frac{4\mathscr{T}^2}{T_0' Ra}U_z^{(0)} = W_r^{(0)} - \frac{Pe'}{T_0'}c_{rz}^{(0)}. \tag{8.6}$$

For convenience in what follows, let $4\mathscr{T}^2/(T_0' Ra) \equiv S^2$. Use of continuity gives the following partial differential equation for the radial velocity component:

$$\frac{\partial}{\partial r}\left(\frac{1}{r}\frac{\partial (rU^{(0)})}{\partial r}\right) + S^2\frac{\partial^2 U^{(0)}}{\partial z^2} = -\frac{Pe'}{T_0'}\frac{\partial^3 c^{(0)}}{\partial z^2 \partial r}. \tag{8.7}$$

To proceed to a solution, we begin by writing the solutal concentration in the same way as in § 5,

$$c_r^{(0)} = \sum_{n=1}^{\infty} \mathscr{C}_n(z) J_1(\alpha_{0n} r), \tag{8.8}$$

and, from substitution, into (8.5*c*), leads to precisely the same result – (6.32), repeated here simply for convenience:

$$\mathscr{C}_n = g_n \mathrm{e}^{-Pe' z/2} \sinh\left(\mathscr{G}_n(L_1 - z)\right), \quad \mathscr{G}_n \equiv \sqrt{\frac{Pe'^2}{4} + \alpha_{0n}^2}. \tag{8.9}$$

Then, the radial velocity can be written as

$$U^{(0)} = \frac{r f_z}{T_0'} + \sum_{n=1}^{\infty} A_n''(z) J_1(\alpha_{0n} r), \tag{8.10}$$

$$A_n'' - \frac{\alpha_{0n}^2}{S^2}A_n = -\frac{r_n f_z}{T_0'} - \frac{Pe'}{T_0'}\mathscr{C}_n, \tag{8.11}$$

where r_n is the Fourier–Bessel series coefficient for the function r. Assuming that the meridional velocity components are fully determined, by solution of (8.11) and use of (8.6), the thermal problem can be posed most usefully in the form

$$\mathscr{D}^2 T_r^{(0)} = T_0' S^2 U_z^{(0)} - Pe' c_{rz}^{(0)}, \tag{8.12}$$

and solving,

$$T_r^{(0)} = \sum_{n=1}^{\infty} B_n'(z) J_1(\alpha_{0n} r), \Longrightarrow \quad B_n'' - \alpha_{0n}^2 B_n = T_0' \alpha_{0n}^2 A_n(z) - S^2 Pe' \mathscr{C}_n(z), \tag{8.13}$$

$$\bar{T}_r^{(0)} = \sum_{n=1}^{\infty} \bar{B}_n'(z) J_1(\alpha_{0n} r), \Longrightarrow \quad \bar{B}_n'' - \alpha_{0n}^2 \bar{B}_n = 0. \tag{8.14}$$

Finally, the swirl velocity is given by

$$V^{(0)} = \frac{2\mathscr{T}^2}{Ra} \sum_{n=1}^{\infty} C_n(z) J_1(\alpha_{0n} r), \quad C_n'' - \alpha_{0n}^2 C_n = \frac{\alpha_{0n}^2}{S^2} A_n(z) - \frac{Pe'}{T_0'} \mathscr{C}_n. \tag{8.15a,b}$$

Actually, not all of these quantities are independent, and it is easily verified that

$$\frac{4\mathscr{T}^2}{Ra} C_n' = B_n' + \mathscr{C}_n. \tag{8.16}$$

8.1.1. *Boundary conditions*

It is immediately evident that $V^{(0)}$ must vanish at $z = 0$ and $z = L_1$, since a non-zero value leads directly from the Ekman suction law to vertical velocities at the Ekman layer edges of $O(Ra^{-3/4})$, which is incompatible with outer scales on the temperature. Hence,

$$V^{(0)}(r, 0) = V^{(0)}(r, L_1) = 0 \Longrightarrow C_n(0) = C_n(L_1) = 0. \tag{8.17}$$

There are the obvious conditions on the temperature at the upper and lower boundaries,

$$B_n'(L_1) = \bar{B}_n'(-L_2) = 0. \tag{8.18}$$

Equation (8.16) then implies that

$$C_n'(L_1) = 0. \tag{8.19}$$

Three conditions derived from the thermal/solutal conditions on the interface delineated in § 2.2, for an interfacial deflection $Z = \mathscr{B}h(r)$ can be put into the form

$$(\bar{T}_0' - MC_0'(0)) T_r^{(0)} - (T_0' - MC_0'(0)) \bar{T}_r^{(0)} = \frac{M}{G} (\bar{T}_0' - T_0') c_r^{(0)} + \Gamma \mathscr{L}^2 [\bar{T}_r^{(0)} - T_r^{(0)}], \tag{8.20}$$

and

$$c_{rz}^{(0)} - (k-1) Pe' c_r^{(0)} = kPe' GC_0'(0) \frac{\bar{T}_r^{(0)} - T_r^{(0)}}{T_0' - \bar{T}_0'}, \tag{8.21}$$

$$T_z^{(0)} = \mathscr{K} \bar{T}_z^{(0)}, \tag{8.22}$$

all to be applied on $z = 0$.

8.1.2. *Toward the outer solution*

To proceed to the solution, it appears simplest to combine (8.11) and (8.15*b*) into a single equation for C_n:

$$\left(\frac{\mathrm{d}^2}{\mathrm{d}z^2}-\frac{\alpha_{0n}^2}{S^2}\right)\left(\frac{\mathrm{d}^2C_n}{\mathrm{d}z^2}-\alpha_{0n}^2C_n\right)=-\frac{\alpha_{0n}^2r_nf_z}{S^2T_0'}-\frac{Pe'}{T_0'}g_n\mathrm{e}^{-Pe'z/2}$$
$$\times\left[\left(\frac{Pe'^2}{2}+\alpha_{0n}^2\right)\cosh\left(\mathscr{G}_n(L_1-z)\right)-Pe'\mathscr{G}_n\sinh\left(\mathscr{G}_n(L_1-z)\right)\right]. \quad (8.23)$$

Three conditions on the solution for C_n are given above in (8.17) and (8.19).

The solution in the solid can be written down with one arbitrary coefficient set, $\{\ell_n\}$, from which we can write

$$\bar{B}_n'(0)=\ell_n\sinh(\alpha_{0n}L_2)-r_nf(-L_2)\cosh(\alpha_{0n}L_2)$$
$$+r_nf(-\bar{z}_I)\cosh(\alpha_{0n}L_2)+\frac{r_nf_z}{\alpha_{0n}}\sinh(\alpha_{0n}L_2), \quad (8.24)$$

and

$$\bar{B}_n''(0)=\alpha_{0n}\ell_n\cosh(\alpha_{0n}L_2)-\alpha_{0n}r_nf(-L_2)\sinh(\alpha_{0n}L_2)$$
$$+r_n\alpha_{0n}f(-\bar{z}_I)\sinh(\alpha_{0n}L_2)+r_nf_z\cosh(\alpha_{0n}L_2). \quad (8.25)$$

Now, the boundary conditions (8.20)–(8.22) at $z=0$ become

$$\left[\mathscr{G}_n\coth(\mathscr{G}_nL_1)+(k+\tfrac{1}{2})Pe'+\frac{kPe'GC_0'(0)}{T_0'-\bar{T}_0'}\right]g_n\sinh(\mathscr{G}_nL_1)$$
$$+\frac{kPe'GC_0'(0)}{T_0'-\bar{T}_0'}\left(\bar{B}_n'(0)-\frac{4\mathscr{T}^2}{Ra}C_n'(0)\right)=0, \quad (8.26)$$

$$\frac{4\mathscr{T}^2}{Ra}C_n''(0)+\left(\frac{Pe'}{2}+\mathscr{G}_n\coth(\mathscr{G}_nL_1)\right)g_n\sinh(\mathscr{G}_nL_1)=\mathscr{K}\bar{B}_n''(0), \quad (8.27)$$

and, finally,

$$\left(\bar{T}_0'-MC_0'(0)-\alpha_{0n}^2\Gamma\right)\frac{4\mathscr{T}^2}{Ra}C_n'(0)=\left(\left[1+\frac{M}{G}\right]\bar{T}_0'-MC_0'(0)-\frac{M}{G}T_0'-\alpha_{0n}^2\Gamma\right)$$
$$\times g_n\sinh(\mathscr{G}_nL_1)+(T_0'-MC_0'(0)-\alpha_{0n}^2\Gamma)\bar{B}_n'(0). \quad (8.28)$$

The solution can now proceed as follows. The solution to equation (8.23) is the sum of the homogeneous solution, with four unknown constants, and a particular solution with multiplier g_n. The quantities $\{\ell_n\}$ are also not known, so that six conditions in total are required. Three of those conditions are given in (8.17) and (8.19) as noted above. Equations (8.26)–(8.28) constitute the other three conditions, involving as they do only $\{C_n(z)\}$ and its derivatives, and the sets of constants $\{g_n,\ell_n\}$.

The complexities of the solution are indeed great, and its completion is not given here.

8.2. *Interfacial boundary layer*

This solution, at $\mathscr{T} = O(Ra^{1/2})$, represents a radical shift in structure from all smaller values of Taylor number in that the boundary layer on the interface is now passive: it plays no primary role in determining the solutal segregation; all of that has been relegated to the outer flow, and as such the segregation has risen in magnitude over that for smaller values of the Taylor number. The surface boundary layer is only an Ekman layer, and we include some details of its solution only for completeness.

The vertical velocity at the interfacial layer's edge is (Ra^{-1}), so that implies the need for the next term in the expansion for v in (8.2) to be $O(Ra^{-3/4})$. Hence, we write, in the interfacial layer, $(u, v) = Ra^{-3/4}(\bar{u}, \bar{v})$, $w = Ra^{-1}\bar{w}$; the boundary-layer coordinate is $z = \mathscr{T}^{-1/2}\bar{z}$. The horizontal momentum equations then have the simple (leading-order) solution

$$\bar{u} + \mathrm{i}\bar{w} = \mathrm{i}\bar{v}_e[1 - \mathrm{e}^{-(1+\mathrm{i})\bar{z}}], \tag{8.29}$$

where $\bar{v}_e$ is the edge velocity. In the usual way, integration of the continuity equation leads to the vertical velocity component in the layer,

$$\bar{w} = \frac{(r\bar{v}_e)_r}{2r}\,\mathrm{Re}\,((\mathrm{i}+1)(1 - \mathrm{e}^{-(1+\mathrm{i})\bar{z}})), \tag{8.30}$$

from which, on matching to the outer expansion, we obtain the relationship

$$W^{(0)} = \frac{1}{2r}\frac{\mathrm{d}(rV^{(1)})}{\mathrm{d}r} \quad \text{at } z = 0. \tag{8.31}$$

The thermal variation in the layer is found by writing

$$T = T^{(0)}|_{z=0} + Ra^{-1/4}T_z^{(0)}|_{z=0}\bar{z} + Ra^{-1/2}[\tfrac{1}{2}T_z^{(0)}|_{z=0}\bar{z}^2 + \bar{T}(r, \bar{z})] + \cdots. \tag{8.32}$$

Then, the equation satisfied by $\bar{T}$ is

$$\bar{T}_{\bar{z}\bar{z}} = T_0'(\bar{w} - \bar{w}_e). \tag{8.33}$$

Integrating twice,

$$\bar{T} = \bar{T}|_{\bar{z}=0} + T_0'\frac{(r\bar{v}_e)_r}{2r}\left[\frac{1}{2} - \frac{1}{\sqrt{2}}\mathrm{e}^{-\bar{z}}\cos(\tfrac{1}{4}\pi + \bar{z}) + \bar{z}(\cos\bar{z} - \tfrac{1}{2}\sin\bar{z})\mathrm{e}^{-\bar{z}}\right]. \tag{8.34}$$

What we see is that, as tacitly assumed in the previous section, there is no change in T across this layer until $O(Ra^{-1/2})$, so that values of T and T_z at the interface are simply the values from the outer flow that penetrate without change through this layer. It is evident, as well, that if one works out the next order terms in the asymptotic series, there is a change in T_z at that level.

Further note that equation (8.31) provides the boundary condition on the second-order outer solution.

Though the final details of the complicated solution in this parameter range are not given here, the qualitative results are important, particularly the scalings summarized in table 1. What has happened at this $\mathscr{T}$ level is that the thermal variations necessary to satisfy the melting conditions at $z = Z$ occur over the entire interior of the melt and are not confined to a thermal boundary layer at the crystal–melt interface, and therefore the concentration and interfacial displacement perturbations are greatly enhanced.

9. Axisymmetric solutions for $\mathscr{T} = O(Ra)$

It appears that the material segregation has increased with $\mathscr{T}$ to $O(\mathscr{B})$, and that increased rotation cannot reduce it. As a final check of that situation, we explore the case for which rotation is truly dominant: $\mathscr{T} = O(Ra)$.

9.1. *The outer expansion*

In this parameter range, the outer expansions take the form

$$\begin{pmatrix} u \\ w \end{pmatrix} = \mathscr{T}^{-3/2} \begin{pmatrix} U^{(0)} \\ W^{(0)} \end{pmatrix} + \mathscr{T}^{-2} \begin{pmatrix} U^{(1)} \\ W^{(1)} \end{pmatrix} + \cdots, \tag{9.1}$$

$$v = \mathscr{T}^{-1} V^{(0)} + \mathscr{T}^{-3/2} V^{(1)} + \cdots, \tag{9.2}$$

$$\begin{pmatrix} T \\ c \end{pmatrix} = \begin{pmatrix} T^{(0)} \\ c^{(0)} \end{pmatrix} + \mathscr{T}^{-1/2} \begin{pmatrix} T^{(1)} \\ c^{(1)} \end{pmatrix} + \cdots. \tag{9.3}$$

Substitution into the equations of motion (2.5)–(2.8) gives the first-order results

$$2V_z^{(0)} = T_r^{(0)} + c_r^{(0)}, \quad U^{(0)} = 0, \quad W_z^{(0)} = 0, \quad \nabla^2 T^{(0)} = 0. \tag{9.4a–d}$$

The usual equation for $c^{(0)}$ is (4.4*c*), and is not written down here.

To next order, we have

$$2V_z^{(1)} = T_r^{(1)} + c_r^{(1)}, \quad U^{(1)} = \mathscr{D}^2 V^{(0)}, \quad \nabla^2 T^{(1)} = T_0' \frac{Ra}{\mathscr{T}} W^{(0)}. \tag{9.5a–c}$$

The boundary layers on $z = Z^+$ and $z = L_1^-$ are Ekman layers, and putting these expansions into the usual Ekman suction law gives

$$W^{(0)} = \mp \frac{1}{2} \frac{1}{r} \frac{\partial}{\partial r} (r V^{(0)}) \quad \text{on} \quad z = 0, L_1. \tag{9.6}$$

Integrating (9.4*a*) in z, from the interface to the top of the ampoule, then utilizing the Ekman conditions (9.6), we have

$$W^{(0)} = \tfrac{1}{2} \left[T_z^{(0)} |_{z=0}^{z=L_1} + c_z^{(0)} |_{z=L_1} - [c_z^{(0)} + Pe' c^{(0)}]_{z=0} \right]. \tag{9.7}$$

Interestingly, it is easily shown from this result that

$$\int_0^{L_1} r W^{(0)} \, \mathrm{d}r = 0 \quad \Longrightarrow \quad V^{(0)}(1, z) = 0. \tag{9.8}$$

The latter result follows directly from (9.6). Interestingly, there is, then, no net vertical transport of fluid in the interior.

So, once the solutions for $T^{(0)}$ and $c^{(0)}$ are complete, the vertical velocity in the core flow can be worked out from (9.7). Slow, vertical flow is characteristic of rotating flows, and, interestingly, drift velocity is here determined solely by the thermal and concentration fields. Once that is known, then the next order thermal perturbation may be found from (9.5*c*). The leading-order swirl is determined from (9.4*a*), then utilized to work out the (slow) radial component from (9.5*b*); in fact, the next order velocity is entirely determined as

$$U^{(1)} = -Pe' c_r^{(0)}, \qquad W^{(1)} = Pe' c_z^{(0)} + Pe'^2 c^{(0)}. \tag{9.9}$$

Writing the interfacial deflection as $Z = \mathscr{B} h(r)$, the usual boundary conditions on the thermal fields take the form

$$(T_0' - \bar{T}_0') h + T^{(0)} - \bar{T}^{(0)} = 0, \qquad T_z^{(0)} = \mathscr{K} \bar{T}_z^{(0)} \quad \text{at } z = 0. \tag{9.10a,b}$$

As we have seen in (9.4) above, $T^{(0)}$ – and of course $\bar{T}^{(0)}$ – are harmonic, subject to these two joining conditions, and

$$T_r^{(0)} = f(z), \quad \bar{T}_r^{(0)} = \bar{f}(z) \quad \text{on } r = 1. \tag{9.11}$$

Of course, the solution cannot be independently completed, since h is not known. The other conditions, involving the concentration field, become

$$(T_0' - MC_0'(0))h + T^{(0)} = \frac{M}{G}c^{(0)} + \Gamma \nabla_h^2 h, \tag{9.12}$$

$$c_z^{(0)} - (k-1)Pe'c^{(0)} = kC_0'(0)GPe'h. \tag{9.13}$$

We proceed now to the solution. Eliminating h among (9.10*a*), (9.12) and (9.13), we obtain the coupled conditions on the thermal and concentration fields,

$$(T_0' - MC_0'(0))\bar{T}_r^{(0)} - (\bar{T}_0' - MC_0'(0))T_r^{(0)} = \frac{M}{G}(T_0' - \bar{T}_0')c_r^{(0)} + \Gamma \mathscr{L}^2(\bar{T}_r^{(0)} - T_r^{(0)}) \tag{9.14}$$

and

$$c_{rz}^{(0)} - (k-1)Pe'c_r^{(0)} = kC_0'(0)GPe'\frac{\bar{T}_r^{(0)} - T_r^{(0)}}{T_0' - \bar{T}_0'}, \tag{9.15}$$

which are to be utilized together with (9.10*b*).

It is convenient to write the solutions in the form

$$\begin{pmatrix} \bar{T}_r^{(0)} \\ T_r^{(0)} \end{pmatrix} = \begin{pmatrix} r\bar{f}(z) \\ rf(z) \end{pmatrix} + \frac{\partial^2}{\partial z^2}\sum_{n=1}^{\infty}\begin{pmatrix} A_n(z) \\ B_n(z) \end{pmatrix} J_1(\alpha_{0n}r). \tag{9.16}$$

The concentration is given again by (8.8) and (8.9).

Substitution of (9.16) into the Laplace equations and solving gives the following rather complicated result for the solute concentration at the solidifying boundary:

$$\mathscr{C}_n(0) = \frac{\alpha_{0n}^2 Gr_n \phi_n}{M(T_0' - \bar{T}_0')} \frac{(\Lambda_n - 1)(\alpha_{0n}^2\Gamma - MC_0'(0)) + T_0'(\Lambda_n - \mathscr{K})}{\mathscr{K}\Lambda_n \sinh(\alpha_{0n}L_1)\cosh(\alpha_{0n}L_2) + \sinh(\alpha_{0n}L_2)\cosh(\alpha_{0n}L_1)}, \tag{9.17}$$

where

$$\begin{aligned}\phi_n = {} & \mathscr{K}\frac{\bar{f}(-\bar{z}_I)}{\alpha_{0n}^2}\cosh(\alpha_{0n}(L_2 - \bar{z}_I))\sinh(\alpha_{0n}L_1) - \mathscr{K}\frac{\bar{f}(-L_2)}{\alpha_{0n}^2}\sinh(\alpha_{0n}L_1) \\ & + \frac{f(z_I)}{\alpha_{0n}^2}\cosh(\alpha_{0n}(L_1 - z_I))\sinh(\alpha_{0n}L_2) - \frac{f(L_1)}{\alpha_{0n}^2}\sinh(\alpha_{0n}L_2) \\ & - \mathscr{K}\frac{\bar{f}'}{\alpha_{0n}^3}\sinh(\alpha_{0n}(L_2 - \bar{z}_I))\sinh(\alpha_{0n}L_1) + \frac{f'}{\alpha_{0n}^3}\sinh(\alpha_{0n}(L_1 - z_I))\sinh(\alpha_{0n}L_2),\end{aligned} \tag{9.18}$$

$$\Lambda_n = \frac{\bar{T}_0' - MC_0'(0) + \alpha_{0n}^2\Gamma + \Phi_n kPe'MC_0'(0)}{T_0' - MC_0'(0) + \alpha_{0n}^2\Gamma + \Phi_n kPe'MC_0'(0)}, \tag{9.19}$$

and

$$\Phi_n = \left[\mathscr{G}_n \coth(\mathscr{G}_n L_1) + \frac{Pe'}{2}(k-1)\right]^{-1}. \tag{9.20}$$

The complexities of this result are more easily penetrable for a special case: $L_1 \equiv L_2, z_I \equiv \bar{z}_I$. In such a case, we have the simpler result

$$\mathscr{C}_n(0) = \frac{\alpha_{0n}^2 Gr_n}{M(T_0' - \bar{T}_0')} \frac{(\Lambda_n - 1)(\alpha_{0n}^2\gamma - MC_0'(0)) + T_0'(\Lambda_n - \mathscr{K})}{(\mathscr{K}\Lambda_n + 1)\cosh(\alpha_{0n}L_1)}$$
$$\times \left[\left(\frac{\mathscr{K}\bar{f}(-z_I)}{\alpha_{0n}^2} + \frac{f(z_I)}{\alpha_{0n}^2} \right) \cosh(\alpha_{0n}(L_1 - z_I)) - \frac{\mathscr{K}f(-L_1)}{\alpha_{0n}^2} \right.$$
$$\left. + \left(\frac{f'}{\alpha_{0n}^3} - \frac{\mathscr{K}\bar{f}'}{\alpha_{0n}^3} \right) \sinh(\alpha_{0n}(L_1 - z_I)) - \frac{f(L_1)}{\alpha_{0n}^2} \right]. \tag{9.21}$$

From this expression, it is evident that no geometrical optimization for long ampoules of the kind found for $\mathscr{T} \equiv 0$ flows (Tanveer 1994; Foster 1997, 1999) is possible here. Essentially, the condition found previously chooses parameters that make $g_1 = 0$. In this expression, the first term in the square bracket is dominant for large L_1, with apparently nothing to balance it; further, its coefficient cannot be zero. A more detailed examination of g_1, inserting the proper expressions for thermal gradients, confirms that conclusion. Nonetheless, lengthening the ampoule, holding other parameters fixed, leads to great improvement. For L_1 and L_2 large,

$$\mathscr{C}_n(0) \sim \frac{Gr_n}{M(T_0' - \bar{T}_0')} \frac{(\Lambda_n - 1)(\alpha_{0n}^2\Gamma - MC_0'(0)) + T_0'(\Lambda_n - \mathscr{K})}{\mathscr{K}\Lambda_n + 1}$$
$$\times \left[\mathscr{K}\bar{f}(-L_2)\mathrm{e}^{-\alpha_{0n}\bar{z}_I} + f(L_1)\mathrm{e}^{-\alpha_{0n}z_I} \right]. \tag{9.22}$$

9.2. *The sidewall boundary layer*

We know that there are two possible layers in these rotation-dominated flows. The outer 'quarter layer' is absent here, however. Doing the usual 'third layer' scalings, we write $r - 1 = \mathscr{T}^{-1/3}\eta$, and the equations of motion take a familiar form

$$\frac{\partial^3 v}{\partial \eta^3} = -2\frac{\partial w}{\partial z}, \qquad \frac{\partial^3 w}{\partial \eta^3} = 2\frac{\partial v}{\partial z} - 2\frac{\partial v_e}{\partial z}, \tag{9.23}$$

where the final term in the second equation is not present in the usual 1/3-layer equation, and is present here because of the 'thermal wind' interior balance. We saw in (9.8) that $V^{(0)} = 0$ at $r = 1$, and because there is no net vertical transport in the interior flow, the first terms in the asymptotic expansion in this boundary layer are $\mathscr{T}^{-3/2}(v^{(0)}, w^{(0)})$.

In a familiar way best exemplified by Moore & Saffman (1969), we integrate the first of these two equations in z to yield

$$\frac{\mathrm{d}^3}{\mathrm{d}\eta^3} \int_0^{L_1} v^{(0)}\,\mathrm{d}z = 0, \tag{9.24}$$

where we have used the Ekman conditions at both $z = 0$ and $z = L_1$, which require that $w^{(0)} = 0$ at both locations. This first term in the layer series matches to $V^{(0)}(1, z)$ in the outer expansion. Integrating (9.24) and matching,

$$\int_0^{L_1} v^{(0)}\,\mathrm{d}z = 0. \tag{9.25}$$

There is no difficulty in working out the solution, which is most easily written down as

$$\frac{w^{(0)}(\eta, z)}{W^{(0)}(1, z)} = 1 - \sum_{n=1}^{\infty} G_n(\eta) \sin\left(\frac{n\pi z}{L_1}\right), \tag{9.26}$$

$$G_n(\eta) = \frac{1-(-1)^n}{2n\pi}\left[e^{\gamma_n \eta} + \cos\left(\frac{\sqrt{3}}{2}\gamma_n \eta\right) e^{\gamma_n \eta/2} + \frac{1}{\sqrt{3}} \sin\left(\frac{\sqrt{3}}{2}\gamma_n \eta\right) e^{\gamma_n \eta/2}\right],$$

$$\gamma_n = \left(\frac{2n\pi}{L_1}\right)^{1/3}. \tag{9.27}$$

The velocity magnitudes for this regime, for Regions IV–VI of figure 2, are entered in table 1.

10. Conclusions

10.1. *Parametric restrictions*

The restrictions on the relative orders of the many parameters in large-Ra Bridgman problems are thoroughly discussed elsewhere (Foster 1997, 1999). The severest restriction is on the Biot number:

$$\mathscr{B} \ll 1. \tag{10.1}$$

However, the solutions presented here, for all the values of $\mathscr{T}$, are proportional to $Q_n'''(0)$, and if the ampoule is long, then $Q_n'''(0)$ scales with $\exp(-\alpha_{mn} z_I)$. Since this factor is multiplicative in all solutions, this 'exponential quenching' due to the insulated zone reduces the small-Biot-number requirement to the much milder one,

$$\mathscr{B} e^{-\alpha_{11} z_I} \ll 1, \quad \text{for } L_1, L_2 \gg 1, \tag{10.2}$$

since α_{11} is the smallest of the zeros of J_m'. Recall, too, from § 2.2.1 that this Biot number is replaced by a modified Biot number when effects of thin, finite ampoule walls are incorporated. Other restrictions have already been noted in (2.9), (2.11) and (2.12).

10.2. *Summary*

As an overview of what happens over the range of Taylor numbers considered here, table 1 evidences a number of interesting patterns arising from the presence of rotation; the two most significant are as follows:

For Taylor numbers larger than $Ra^{1/6}$, the distinction between Regions V and VI in figure 2 begins to disappear, as swirl motion arises throughout the melt. Real structural changes in the thermal field arise at still larger Taylor numbers, of order $Ra^{1/2}$ and larger: at smaller Taylor numbers, the interior balance in the melt is hydrostatic – which strongly constrains the flow-field structure; as the Taylor number builds, eventually a 'thermal wind' balance replaces the simpler hydrostatic constraint when $\mathscr{T} = O(Ra^{1/2})$, generating further mixing in the melt across its entire height. Thus, the rotation eliminates the upper- and lower-eddy flow structure familiar in other works. (See Ardonato & Brown 1987, for example.)

The 'thermal layer' begins to thicken at $\mathscr{T} = O(Ra^{1/3})$, giving rise to larger interfacial deflection and larger lateral dopant gradient for this and larger $\mathscr{T}$.

The evolution of the flow fields and solidification pattern with $\mathscr{T}$ may be understood in a general fashion that makes it possible to anticipate what stirring methods have

a chance of improving segregation. The solutal distribution at the interface, which freezes into the crystal, is governed to leading order by heat flux from below (Region VII) into the melt. That flux is always $O(\mathscr{B})$, so that means that $\partial T/\partial z$ in the melt, near $z = Z^+$, must be of the same order. For all $O(Ra^{1/3})$ Taylor numbers, that layer has width $Ra^{-1/6}$, so the thermal (and solutal) perturbation must be $O(\mathscr{B}Ra^{-1/6})$ in the layer. However, as we saw in § 7, for $\mathscr{T}$ in the range between $Ra^{1/3}$ and $Ra^{1/2}$, the layer across which the temperature has a non-trivial variation fattens to a width of $\mathscr{T}/Ra^{1/2}$, thus making the lateral concentration gradient larger, up to $O(\mathscr{B}\mathscr{T}/Ra^{1/2})$. Once $\mathscr{T}$ reaches $O(Ra^{1/2})$, as delineated in § 8, the thermal variations occur on outer scales – even though there is still a velocity boundary layer on the interface. Since the z scale has become $O(1)$, the thermal perturbation is now $O(\mathscr{B})$.

We can now anticipate that for any stirring technique (like ACRT, for example, in Moon *et al.* 1997) to improve segregation, the interfacial boundary layer must be thinner than $Ra^{-1/6}$, or the structure at that layer must be dramatically altered in a way that changes the interfacial concentration.

Clearly, in the case of the addition of rigid rotation examined here, we verify what has been recently reported in a numerical study by Lee & Pearlstein (1998): there is no reduction in crystalline segregation with rotation. In fact, large rotation makes it worse! However, the thickening of the interfacial layer may indeed, as Weber *et al.* (1990) have indicated, delay the onset of some interfacial instabilities to larger Rayleigh numbers. That matter is discussed briefly in § 10.3.

Weber *et al.* (1990) examined the changes in performance in a situation for which the rotation vector is at right angles to the vertical Bridgman axis. A preliminary investigation of that situation shows no real improvement of the solutal distribution, at least for $Ra \gg 1$. However, it appears that rotating at an angle to the vertical axis (Weber *et al.* 1990; Friedrich *et al.* 1996) is a different matter: such a configuration seems to increase the isolation of the upper and lower eddies – rather than decreasing that isolation as it does for the geometrical arrangement studied here – so there is hope that the overall performance may improve. Analysis of that situation will be reported subsequently.

Optimization conditions found by Tanveer (1994) remain valid for all Taylor numbers less than $Ra^{1/2}$. However, beyond that value of $\mathscr{T}$, we have seen that no such optimization is possible.

Finally, the rotation rates considered here in the various parameter regimes are actually quite low. If the Rayleigh number is 10^9, for example, for typical alloys in an ampoule one or two centimetres in radius, the rotation rates corresponding to $\mathscr{T} = O(Ra^{1/3})$ are between 2 and 5 r.p.m.

10.3. *Effects on morphological instability*

We noted in the introduction that Weber *et al.* (1990) suggest that Coriolis effects might improve interfacial stability. It turns out in the case of the Bridgman solutions that the neutrally stable condition is given by the zero of the denominator of the expression for the surface concentration gradient, c_r, or the interfacial deflection gradient, h_r. Foster (2000) has found that the stability condition comes directly from (4.21) for the no-rotation case, and is

$$\frac{T_0'}{MC_0'(0)} > 1 - \frac{kPe'(1+G/M)}{\mathscr{G}_n + (k-\frac{1}{2})Pe'} - \frac{\alpha_{0n}^2\Gamma}{MC_0'(0)}\left[1 - \frac{kPe'}{\mathscr{G}_n + (k-\frac{1}{2})Pe'}\right], \tag{10.3}$$

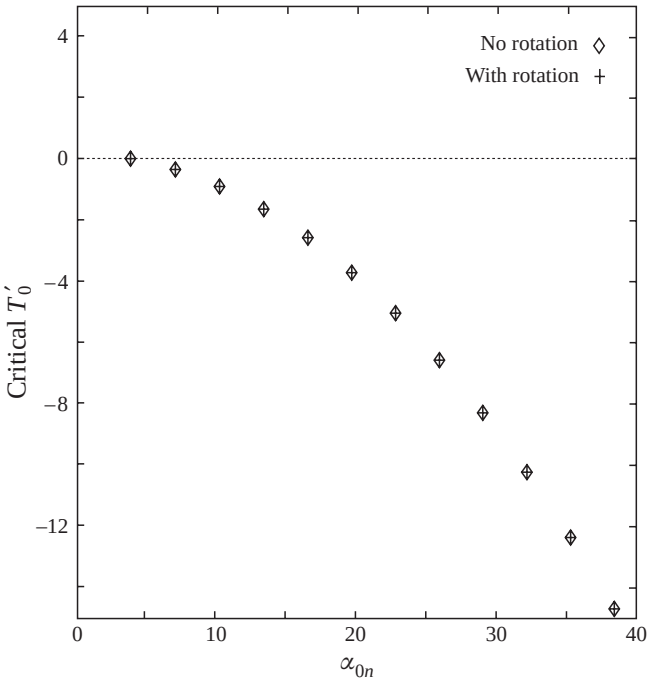

FIGURE 4. For stability, T_0' must be larger than any value on the curve, depending on whether or not rotation is present. The parameters are $Pe' = 0.15$, $\mathscr{K} = 1$, $M = G = -1$, $k = 0.10$ and $\Gamma = 0.01$.

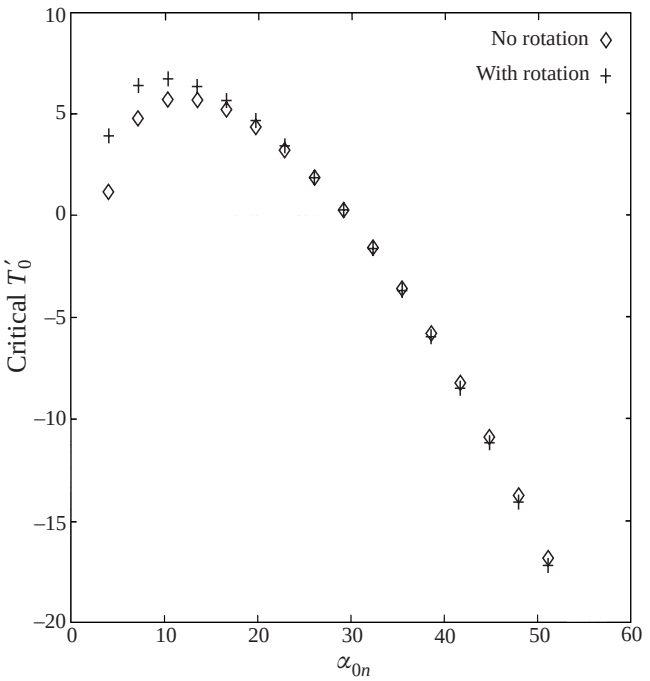

FIGURE 5. As figure 4 but for $Pe' = 10.0$.

for axisymmetric modes only; the notation is that of § 4.1. Clearly, for stability, this inequality must be satisfied for any n. The quantity on the left-hand side can be rewritten as

$$\frac{\mathscr{K}}{L_2 + \mathscr{K} L_1} \frac{\Delta T}{(1-k)m\Delta c^*} \frac{D}{Va}, \tag{10.4}$$

so this requirement puts an upper limit on the pulling speed in the device, as is well known. On the other hand, with significant effects of rotation, results from § 5, in particular the zero of the denominator of (9.17), leads to a different criterion for stability:

$$\frac{T_0'}{MC_0'(0)} > \frac{\mathscr{K}+1}{\mathscr{K}^2+1}\left[1 - \frac{kPe'}{\mathscr{G}_n + \frac{1}{2}Pe'(k-1)} - \frac{\alpha_{0n}^2 \Gamma}{MC_0'(0)}\right], \tag{10.5}$$

for long ampoules.

The critical T_0' values are shown in figures 4 and 5. For a given apparatus, T_0' must be larger than any data point in the figures to guarantee stability. Note that at small Péclet number, there is virtually no change in the stability behaviour – so stability seems guaranteed for all T_0' with or without rotation. At larger pulling speeds (larger Pe'), a stable interface at a particular value of T_0' may in fact be destabilized with rotation! Hence, from this cursory and admittedly preliminary result, it appears that adding rotation does not permit larger pulling speeds.

REFERENCES

Adornato, P. M. & Brown, R. A. 1987 Convection and segregation in directional solidification of dilute and non-dilute binary alloys: effects of ampoule and furnace design. *J. Cryst. Growth* **80**, 155.

Brattkus, K. & Davis, S. H. 1988 Directional solidification with heat losses. *J. Cryst. Growth* **91**, 538.

Foster, M. R. 1997 Asymptotic analysis of a vertical Bridgman furnace at large Rayleigh number. *Phys. Fluids* **9**, 683.

Foster, M. R. 1999 Asymptotic analysis of a three-dimensional Bridgman furnace at large Rayleigh number. *Phys. Fluids* **11**, 1827.

Foster, M. R. 2000 Morphological instability in a vertical Bridgman furnace at large Rayleigh number. In preparation.

Friedrich, J., Baumgartl, J., Leister, H.-J. & Müller, B. 1996 Experimental and theoretical analysis of convection and segregation in vertical Bridgman growth under high gravity on a centrifuge. *J. Cryst. Growth* **167**, 45.

Greenspan, H. 1964 *The Theory of Rotating Fluids.* Cambridge University Press.

Jalics, M. K. 1998 Numerical treatment of crystal growth in a vertical Bridgman device. PhD Dissertation, The Ohio State University, Department of Mathematics.

Lee, H. & Pearlstein, A. 1998 Effect of rotation on interface shape in Bridgman solidification of benzene. *Bull. Am. Phys. Soc.* **43**, 2109.

Moon, S. J., Kim, C.-J. & Ro, S. T. 1997 Effects of buoyancy and periodic rotation on the melt flow in a vertical Bridgman configuration. *J. Cryst. Growth* **40**, 2105.

Moore, D. W. & Saffman, P. G. 1969 The structure of the free vertical shear layers in a rotating fluid and the motion produced by a rising body. *Phil. Trans. R. Soc. Lond.* A **264**, 597.

Stewartson, K. 1966 On almost rigid rotations. Part 2. *J. Fluid Mech.* **26**, 131.

Tanveer, S. 1994 Convection effects on radial segregation and crystal melt interface in vertical Bridgman growth. *Phys. Fluids* **6**, 2270.

Tanveer, S. 1995 Large solutal Rayleigh number limit in vertical Bridgman crystal growth. Unpublished notes.

Tiller, W. A., Jackson, K. A., Rutter, J. W. & Chalmers, B. 1953 The redistribution of solute atomes during solidification of metals. *Acta Metallurgica* **1**, 428.

Vompe, D. A. 1997 Numerical modeling of crystal growth in Bridgman device, PhD Dissertation, The Ohio State University, Department of Mathematics.

Weber, W., Neumann, G. & Müller, G. 1990 Stabilizing influence of the Coriolis force during melt growth on a centrifuge. *J. Cryst. Growth* **100**, 145.

Xiao, Q. S., Kuppurao, A., Yeckel, A. & Derby, J. 1996 On the effects of ampoule tilting during vertical Bridgman growth: three-dimensional computations via a massively parallel, finite element method. *J. Cryst. Growth* **167**, 292.